



Original Paper

Gravity Modeling of the Au–U Mineralized Crust at the North-Central Cameroon Illustrating Crustal Permeability

Jean Marcel Abate Essi,^{1,2,6} Jean Marcel,^{3,4} Diab Ahmad Diab,⁵
Joseph Quentin Yene Atangana,² Monique Abossolo Angue,² and Joseph Mvondo Ondo²

Received 4 January 2019; accepted 1 June 2019
Published online: 10 June 2019

The north-central Cameroon is located at the northern edge of Archean Congo–Sao Francisco craton and at the east of the West African craton. This area includes various Neoproterozoic to Holocene geological litho-structural units. It corresponds to a juvenile crust resulting from the collision of the above cratons. Geological features associated with the Poli–Ounianga–Kebir heavy gravity line trending NE–SW crosscuts the study area and hosts several deposits, chiefly auriferous and uraniferous ore deposits. Uraniferous bodies are described at the SW and NE sides of the Benue Trough and are related to hydrothermal processes and structural events in Neoproterozoic granitoids of Poli (Cameroon) and Zabili (Chad). Gold ore deposits are found around faulted zones mostly in the Tcholliré shear zone. Gravity data derived from the Earth Gravitational Model EGM2008, combining terrestrial, maritime and satellite-derived data, were used to model the crust of the north-central Cameroon. The geophysical filtering enabled to highlight that the most fractured areas with the deepest faults are situated on the positive anomalies of the mineralized volcano-sedimentary belts of Poli and Bibémi. The Benue Trough that crosscuts the volcano-sedimentary belts exposes few structural features due to the weak gravity signal of Cretaceous sedimentary cover. The radially averaged power spectrum analysis brought out the density contrast depths of some geological belts and revealed the Moho discontinuity of the study area at about 24 km depth. This Moho depth is in accordance with the assumption of a thin crust and a mantle upwelling in the study area proposed by previous works. Thus, the presence of geological formations of mantle, crustal and mixed crustal-mantle origin such as mafic rocks as well as calc-alkaline to alkaline granitoid outcropping in the study area may be the consequence of the proximity of the upper mantle to the surface. Moreover, fractures highlighted in this work brought out the crustal permeability in the study area illustrating migratory passages for mantle formations found at the surface. Based on the gravity field analysis, the proposed models of basement in this study provide geological architecture highlighting the presence of more or less dense rocks and hydrothermal fluids migration along faults as key elements for ore deposits formation.

KEY WORDS: Mineralized crust, Gravity modeling, Faults, Crustal permeability, North-central Cameroon.

¹Institute for Geological and Mining Research, P.O. Box 4110 Nlongkak Yaoundé, Cameroon.

²Department of Earth Sciences, Faculty of Sciences, University of Yaoundé I, P.O. Box 812 Yaoundé, Cameroon.

³National Institute of Cartography, P.O. Box 157 Yaoundé, Cameroon.

⁴Department of Physics, Faculty of Sciences, University of Yaoundé I, Yaoundé, Cameroon.

⁵Department of Physics, Adam Barka of Abeche University, Abeche, Chad.

⁶To whom correspondence should be addressed; e-mail: abatemarcel@yahoo.fr

INTRODUCTION

The major geological features of Cameroon are given by an Archean Congo craton (CC) and the Neoproterozoic Central African Fold Belt (CAFB), which are crosscut by the Cenozoic volcanic formations of the Cameroon Volcanic Line and covered in places by sedimentary basins dated back from Mesozoic to Holocene (Eno Belinga 1984; Toteu et al. 2008). The study area is located at the northern edge of CC within the CAFB (Fig. 1). This sector of northern Cameroon is also known as “north-central

Cameroon” (Pinna et al. 1994; Toteu et al. 2001; Bouyo et al. 2015a). Previous works (Toteu et al. 2001; Van Schmus et al. 2008) match the CAFB with the Borborema province (BP) of the NE Brazil. Thus, some common geological features are found in both Central domain of BP (Pernambuco-Alagoas and Transverse domains) and CAFB (Adamawa-Yadé and NW Cameroon domains, Eastern Nigeria terrane). Several geophysical surveys have been carried out in this part of the CAFB. The main regional in situ gravity surveys in Central Africa were performed by ORSTOM (Office de la Recherche Scientifique et Technique d’Outre-Mer, France:

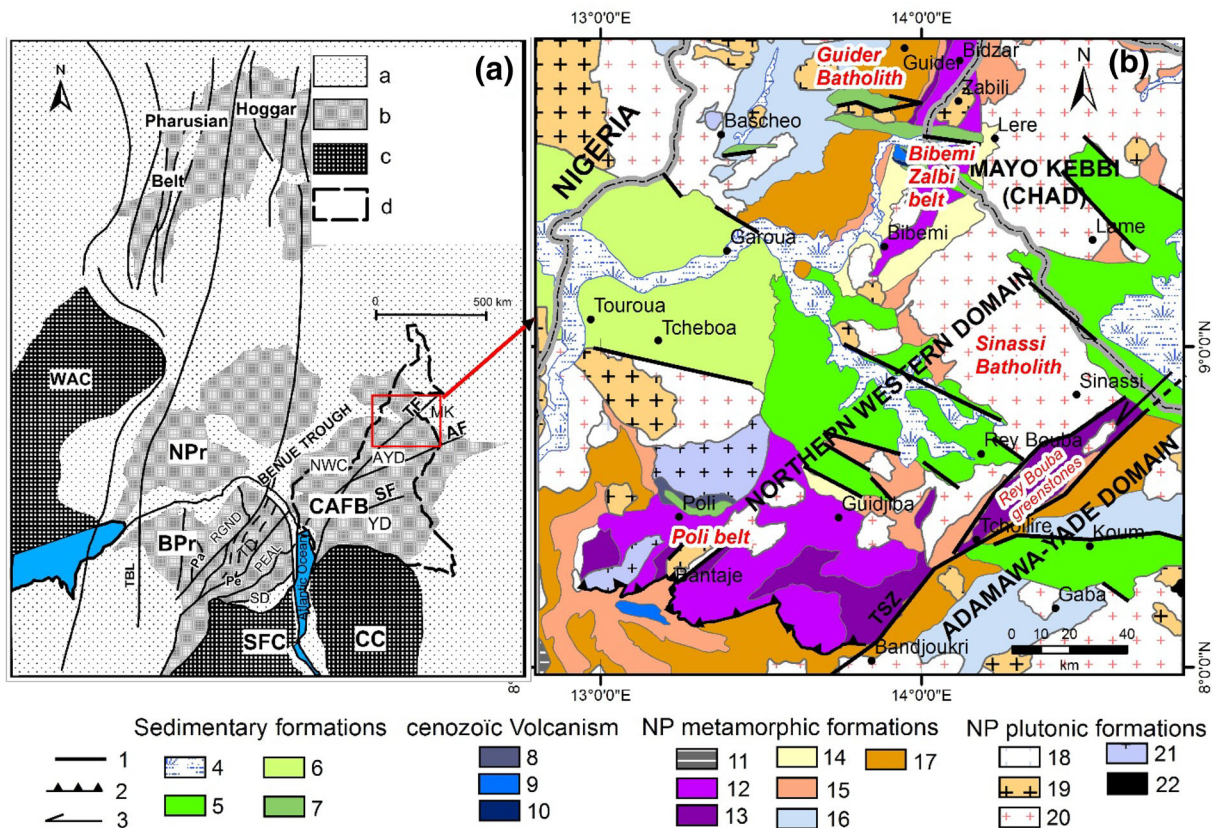


Figure 1. Geological map of the study area (modified from Koch 1959; Schwoerer 1962; Caby 1989; Maurin and Guiraud 1990; Penaye et al. 2006; Van Schmus et al. 2008; Abate Essi et al. 2017): **A** Regional location of the north-central Cameroon on the West Gondwana including west-central Africa and northeast Brazil; **B** Geological sketch map of the study area. Major domains and regions used in **A**: a: Phanerozoic Braziliano-Pan-African sediments. b: Paleo to Neoproterozoic Braziliano-Pan-African Belt; c: Archean cratons d: Cameroon Boundary; WAC: West African craton; SFC: Sao Francisco craton; CC: Congo craton; NPr: Nigerian Province; BPr: Borborema province; PEAL: Pernambuco-Alagoas domain; RGND: Rio Grande do Norte domain; SD: Sergipano domain; TD: Transverse Domain; NWC: Northern Western Cameroon; AYD: Adamawa-Yadé domain; YD: Yaoundé domain MK: Mayo Kebbi. Faults and shear zones used in **(A)**: AF: Adamawa fault; Pa: Patos fault zone; Pe: Pernambuco fault zone; SF: Sanaga fault; TF, Tcholliré fault; TBL: Transbrasiliano lineament. Detailed geology of the study area: NP: Neoproterozoic; TSZ: Tcholliré shear zone. c: craton. 1: Fault. 2: Thrust. 3: Sinistral strike slip fault. 4: Quaternary alluvium. 5: Cretaceous Benue Sandstone. 6: Cretaceous Garoua Sandstone. 7: Divers Cretaceous sediments. 8: andesitic type. 9: acidic type. 10: mafic type. 11: Amphibolite. 12: Upper Mica Schist. 13: Lower Mica Schist. 14: Upper gneiss. 15: Lower gneiss. 16: Migmatitic gneiss. 17: Embrechitic gneiss. 18: Post-tectonic granitoid. 19: Syn to post-tectonic granitoid. 20: Pre- to syn-tectonic granitoid. 21: gabbro. 22: syenite.

Collignon 1968, 1969; Poudjom 1993). Louis (1970) identified a chain of positive gravity anomalies trending NE–SW extending from Cameroon to Chad. He named this chain the “Poli–Ounianga–Kebir heavy line.” Abate Essi et al. (2017) later revealed that auriferous and uraniferous mineralizations line up on this heavy gravity line notably in the study area (Fig. 2). Furthermore, diverse mineral commodities such as gold, uranium and copper are found in the north-central Cameroon. Interesting concentrations (up to 33 g t^{-1}) of gold are described from autochthonous primary and allochthonous alluvial sources (Kusnir 1995; Kusnir and Moutaye 1997; Embui et al. 2013; Tchameni et al. 2013), which can explain the intense artisanal mining activities in the study area. According to Kouske et al. (2012) and Mbagedje (2015), fractures/faults are favorable for hydrothermal fluid migration and the precipitation of gold and uranium in and around the study area. In Pala locality (Chad), Tchameni et al. (2013) suggest that magmatism played a major role in the dynamics of the mineralized fluids in the setting of gold deposit.

Crustal permeability is an important element for hydrothermal and mineralized fluid migration both for igneous rocks like granite and supracrustal sequences such as volcano-sedimentary belts (Tenthorey and Fitz Gerald 2006; Lawther et al. 2016). Faure et al. (2009) and Faure (2010) demonstrated the importance of potential field data to investigate crustal permeability of orogenic gold and uranium in Abitibi (Canada). The modeling of the subsurface using potential field data is very interesting for proposing the geological architecture of the crust based on density contrast (gravity data) and/or susceptibility (magnetic data) of its components. For example, Chicharro et al. (2015) used gravity data to model Logrosán Sn–(W) ore deposits (Central Iberian Zone, Spain) and proposed comprehensive geological and metallogenic contexts for the setup of these ore deposits. Likewise, Fan et al. (2014) used the modeling technique of potential field to study the iron deposit of the Anshan area (China). In this work, we interpret gravity data combined with geological information to propose gravity modeling that may support the development of gold and uranium

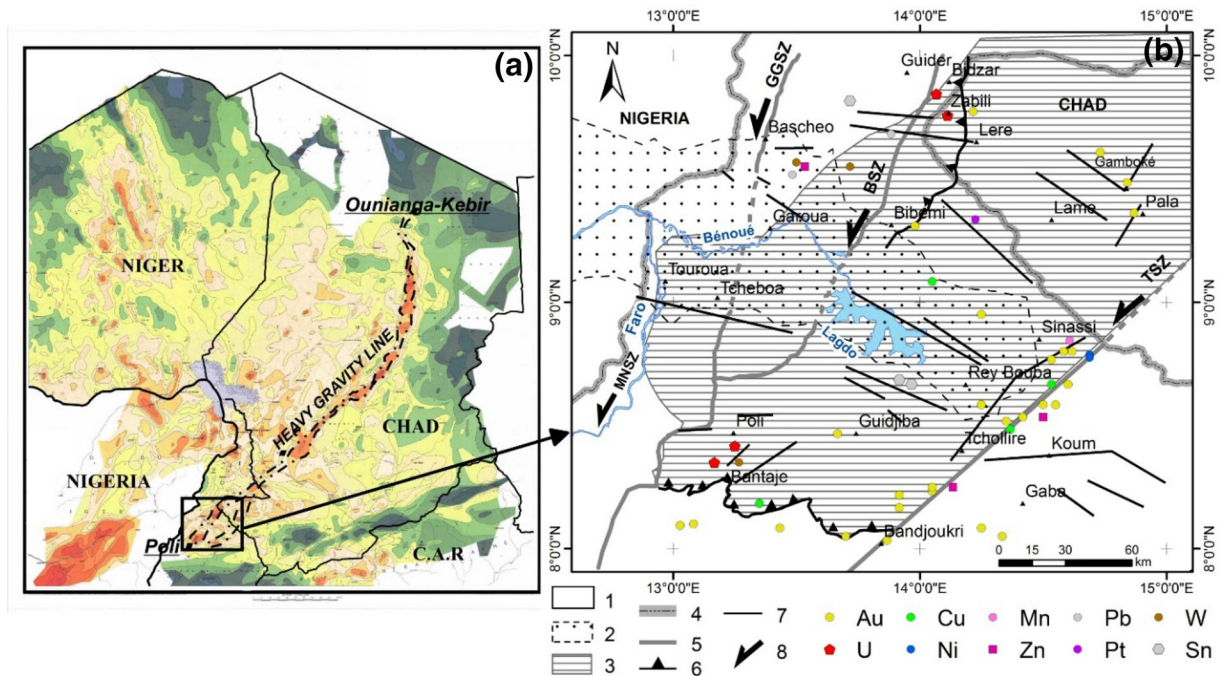


Figure 2. a Chado-Cameroonian heavy gravity line. High-amplitude anomalies are colored in red (+ 30 to – 20 mGal), medium amplitude in green (– 19 to – 60 mGal), low amplitude in yellow (– 59 to – 100 mGal), and very low amplitude (below – 100 mGal) in blue. b Mineral commodities distribution along the heavy gravity line in the north-central Cameroon (modified from Louis 1970; Ngako et al. 2008; Abate Essi et al. 2017). BSZ: Balché shear zone; TBZ: Tcholliré shear zone, GGSZ: Godé–Gormaya shear zone. 1: Neoproterozoic basement. 2: Phanerozoic Benue Trough sediments. 3: country boundaries border. 4: heavy gravity line. 5: strike slip fault. 6: thrust front. 7: faults. 8: sense of wrench movement.

enrichment of the crust in north-central Cameroon. The study area is poorly covered by ground gravity data. We used the Earth gravitational Model EGM2008 (Pavlis et al. 2008, 2012) high-resolution gravity data, to overcome the absence and sparseness of ground data in the study area.

GEOLOGICAL, STRUCTURAL AND MINING BACKGROUNDS

The study area is a part of the mobile belt of Central Africa. It is situated at the northern edge of Congo–Sao Francisco craton and at the east of the West African craton (Fig. 1A). It belongs to two main litho-structural domains of the Neoproterozoic CAFB: the North Western (NW) Cameroon and Adamawa-Yadé (AY) domains. These two domains (Fig. 1B) are separated by the sinistral Tcholliré shear zone (TSZ) at the southeastern edge of the Poli–Ounianga–Kebir heavy gravity line (Abate Essi et al. 2017), and they extend in the southwestern Chad as Mayo Kebbi domain (Louis 1970; Penaye et al. 2006). Table 1 summarizes the main lithologies and the associated mineral commodities in the study area.

North Western (NW) Domain

The NW domain is located at the northwestern side of the TSZ (Fig. 1B). It mainly includes metamorphic, volcano-sedimentary and granitoid formations grouped into belts, namely Poli, Rey Bouba and Bibémi-Zalbi belts (Ngako et al. 2006).

The Poli belt is interpreted as an early back-arc orogenic basin that was formed during 700–665 Ma (Pinna et al. 1994; Toteu et al. 2006; Penaye et al. 2006). It comprises metasedimentary (volcanogenic clastic and/or reworked clastic rocks) and metavolcanic (sodic rhyolites and tholeiitic basalts) units (Njel 1986; Toteu et al. 2006). Structurally, Ngako et al. (1989), Pinna et al. (1994) and Toteu et al. (2004) described a poly-phased tectono-metamorphic evolution marked by an early D1 tectonic nappe deformed by a sub-vertical foliation D2. At Kitongo near Poli locality, Oesterlen and Vetter (1986) and Kouske et al. (2012) revealed that uranium mineralization is hosted in albitized granite. These last authors concluded that most promising uraniumiferous bodies are intimately related with fault intersections rather than along individual faults. This

suggests that these faulted zones, which are dilatational in nature, were highly permeable and that the hydrothermal fluids ponded there could have precipitated uranium therein. Therefore, uranium mineralization (Fig. 2) was controlled by structural and hydrothermal (albitization) events. Moreover, Laplaine (1968), Le Fur (1971) and Toteu et al. (2008) indicated enrichment of gold, copper and silver in the Poli belt.

The Rey Bouba belt is made up mainly of greenstones and batholiths. The Sinassi batholiths, which belong to the Rey Bouba belt, consist mainly of tonalite–trondhjemite–granodiorite (TTG) suite and more or less deformed granites. Penaye et al. (2006) and Bouyo et al. (2015a) revealed that the batholiths of Sinassi (Cameroon) and Mayo Kebbi (Chad) are unique. These batholiths are associated with Rey Bouba, Bibémi-Zalbi and Mayo Kebbi greenstones. The Rey Bouba greenstones, which consist of greenschist facies mafic to felsic volcanic, volcano-sedimentary and sedimentary formations, are associated with TSZ. Gold mineralizations are observed on late fracture zones (Pinna et al. 1989) released in stream sediments. In this area, Embui et al. (2013) estimated gold concentration at 1.12 g t^{-1} , while Pinna et al. (1989) found values greater than 2.79 g t^{-1} . Other mineral commodities (Fig. 2) are reported in previous works of Laplaine (1968) and Toteu et al. (2008).

The Bibémi-Zalbi belt is a greenstone belt (Pinna et al. 1994; Pouclet et al. 2006; Isseini 2011; Mbagedje 2015) consisting of (1) ultramafic rocks cropping out as talc schists or serpentinites, (2) metavolcanic and metasedimentary formations and (3) a meta-plutonic complex. These rock units are intruded by post-tectonic granitoids (Zabili granite, Pala hypersthene monzodiorite and porphyritic granite) (Penaye et al. 2006). The Bibémi-Zalbi and Poli belts have some petrographic, structural and geochronological similarities. The Yola–Garoua branch of the Benue Trough that separates them. The Yola–Garoua branch resulted from the opening of the Atlantic Ocean during lower Cretaceous (Reyment and Dingle 1987). It is filled by sandstones distinguished as “Garoua sandstone” and “Benue sandstone” (Shwoerer 1962; Benkhelil 1986) associated with plutonic intrusions and volcanism. In Gamboke near Pala locality (Mayo Kebbi domain, Chad), gold mineralization is described in quartz veins associated with sulfur in a NE-trending shear zone (Kusnir and Moutaye 1997; Mbagedje 2015). Besides, in Zabili near Zalbi (Chad), the uranium

Table 1. Synoptic table of mineral commodities with geology of study area. TTG: tonalite–trondhjemite–granodiorite, MIC: mafic to intermediate complex

Geological Group	Main lithologies	Principal mineral (and locality)	Associated minerals	References
Volcano-sedimentary formations (NW Domain)				
Poli belt	Metasedimentary and metavolcanic rocks Medium-tohigh-grade gneisses Tholeiitic Basalts Calc-alkaline rhyolites Conglomeratic sedimentary sequences	Gold Copper (Bantaje)	U, W, Cu, Mo W, U, Mo, Au	Laplaine (1968), Le Fur (1971), Njel (1986), Ngako et al. (1989), Angoua et al. (2008) and Toteu et al. (2008)
Rey Bouba belt (Tcholliré and Rey Bouba)	Metapelites and meta-graywackes Mafic volcanic rocks (dacitic tuff) Coarse conglomerates TTG	Gold Nickel Copper	Ag, Cu, Mn, Zn, W, P, Pb, As Mn, As, Au, Co Au	Laplaine (1968), Pinna et al. (1989, 1994), Toteu et al. (2008), Embui et al. (2013) and Bouyo et al. (2015b)
Bibémi-Zalbi Belt	Calc-alkaline tholeiitic meta-basalts, Metadolerites, meta-graywackes, Chloritochists, meta-cherts and meta-carbonates, talc schists and serpentinites, MIC (amphibolites, meta-gabbros and meta-diorites)	Platinum (Bibémi) Graphite (Mayo Loue) Lead (Ribao) Zinc (Goutchomi) Gold	W, Zn, Al	Laplaine (1968), Toteu et al. (2008), Kusnir and Moutaye (1997), Toteu et al. (2008), Isseini (2011), Tchameni et al. (2013), Mbagedje (2015) and Diab (2016)
Granitic formations (NW domain)				
Poli Granitoid	Pre- to post-tectonic calc-alkaline granitoids (diorites, granodiorites and granites)	Gold (Faro) Tin (Hosser Nyore) Uranium (Kitongo)	Sulfur pyrite, galena (lead sulfide)	Laplaine (1968), Oesterlen and Vetter (1986), Pinna et al. (1989, 1994), Toteu et al. (2008) and Kouske et al. (2012)
Sinassi (Rey Bouba) Batholith	TTG, orthogneiss, high-grade gneiss	Gold	Ag, Cu	Laplaine (1968), Pinna et al. (1989), Penaye et al. (2006), Toteu et al. (2008), Bouyo et al. (2015a)
Pologozom Batholith	Post-tectonic alkaline granitoids (granites, syenites)	Lead (Goutchoumi) Tin (Peske Bori)	W, Zn,	Toteu et al. (2008), Dawai (2014) and Dawai et al. (2013)
Mayo Kebbi Batholith	TTG (granites, diorites, granodiorites and charnockites) Enclaves of amphibolites	Uranium (Zabibili) Gold	Cu, Pb	Kusnir and Moutaye (1997), Tchameni et al. (2013), Isseini (2011), Mbagedje (2015) and Diab (2016)
Adamawa-Yadé domain				
Ngaoundéré-Mbé Belt	Orthogneiss (biotite-amphibole gneiss, amphibole-pyroxene gneiss and amphibolites), meta-sediments (metapelites and meta-graywackes) syn to post-tectonic granitoids	Gold	Ag, Cu	Laplaine (1968), Toteu et al. (2001) and Tchameni et al. (2013)

mineralization was formed during syn- to post-magmatic ductile to brittle deformation of a granite with metasomatic alteration. Fluid circulations should influence Na-metasomatism and be responsible for the mobilization, transfer and deposition of

uranium and other associated elements (Mbagedje 2015).

The Guider-Boussoum-Pologozom batholith thrusts westward Bibémi-Zalbi belt. Considering its characteristics, the Guider-Boussoum-Pologozom

batholith is similar and coeval to Nigerian eastern plutons. It is composed of syenite, granite associated with orthogneiss with foliation trending NNE–SSW to NE–SW (Dawai 2014), in accordance with the Godé–Gormaya shear zone (GGSZ). In this zone, Ngako et al. (2008) described the GGSZ as a synthetic sinistral shear zone coeval with the TSZ with similar metamorphic evolution. Based on structural field data, they suggested that this shear zone is marked by a successive compressional and extensional evolution.

Adamawa-Yadé (AY) Domain and Intra-continental Sedimentary Basins

The AY Domain is located on the SE side of the TSZ and is interpreted as a Palaeoproterozoic crust that was dismembered during the Pan-African orogeny (Fig. 1B). It comprises (1) dominantly granitoid rocks and (2) lesser metasedimentary formations and orthogneisses. Auriferous minerals are identified on granitoids and gneisses of Bandjougri locality (Van Schmus et al. 2008; Toteu et al. 2008). The minor intra-continental basin of Koum is identified therein. This Cretaceous sedimentary basin consists of conglomerates, sandstones, shales, marlstones with fossils, and it is interpreted as being part of both the West and Central African Rift Systems (Nolla et al. 2015).

Several gold deposits are identified around the TSZ and surrounding localities such as Mbé, Gamba, Landou, Tcholliré and Bandjougri (Laplaine 1968; Pinna et al. 1989; Toteu et al. 2008; Tchameni et al. 2013). According to Tchameni et al. (2013), the TSZ was a major conduit for auriferous fluids and it is comprised most likely of late Pan-African shear structures, developed in the CAFB. They indicated some gold-bearing quartz veins with NW–SE or N–S to NNE–SSW directions, which correlate with regional strike slip shear zones trending NE–SW, similar to the TSZ.

DATA

Gravity data derived from the Earth Gravitational Model EGM2008 were used in this work. The EGM2008 model, which is an improved version of the Earth Gravitational Model EGM96, was released by the National Geospatial Intelligence Agency. It is a spherical harmonic model of the

gravitational potential from the Earth, complete to degree and order 2159, with additional coefficients up to degree 2190 and order 2159 (Pavlis et al. 2008, 2012). The EGM2008 model integrates surface (terrestrial, maritime and airborne) gravity data and satellite altimetry-derived data with an initial spatial resolution of 5 arcmin. This high-spatial resolution model is more spread than terrestrial gravity data and therefore overcomes the sparseness and the absence of terrestrial data (Eyike et al. 2010; Abate Essi et al. 2017; Marcel et al. 2018a, b).

Bouguer corrections were performed at the Bureau Gravimétrique International (BGI). Bouguer and free air (Fig. 3) anomalies were computed from EGM2008 spherical harmonic coefficients through the FA2BOUG program (Fullea et al. 2008) on a grid averaged over 2.5 arcmin by 2.5 arcmin. The topographic correction was performed using the digital elevation data ETOPO1 (Amante and Eakins 2008) with 1 arcmin by 1 arcmin spatial resolution and up to a distance of 167 km (Fig. 4). The density reduction for Bouguer anomaly used was 2.67 g cm^{-3} .

Minimum curvature was used as gridding method to produce free air (Fig. 3) and Bouguer (Fig. 5) anomaly maps with grid cell size of 0.01° (about 1.1 km). This same grid cell size has been successfully experimented by Ngatchou et al. (2014) and Marcel et al. (2018a) to investigate crustal structure beneath Cameroon and subsurface of the Cameroon Volcanic Line, respectively. Moreover, several other works demonstrated the efficiency of EGM2008-derived gravity data in geological and geophysical explorations (Eyike et al. 2010; Abate Essi et al. 2017; Yushan and Yuanyuan 2017; Marcel et al. 2018b).

The EGM2008-derived free air anomaly map of the study area (Fig. 3) exposes values ranging between -26 and 83 mGal . This map brings out the main geological features highlighted by previous studies (Penaye et al. 2006; Toteu et al. 2008; Abate Essi et al. 2017). Sedimentary basins appear as negative anomalies, while magmatic and metamorphic formations are distinguished by high-to-medium-amplitude anomalies. In the Garoua–Rey Boubou sector, a negative anomaly oriented NE–SW represents the Yola–Garoua branch of the Benue Trough (Benkhelil 1986), which is filled with low-density sandstones. This corridor of negative anomalies crosscuts the heavy gravity line (Louis 1970) represented by the two positive anomalies of Poli and Bibémi. Furthermore, the other intra-con-

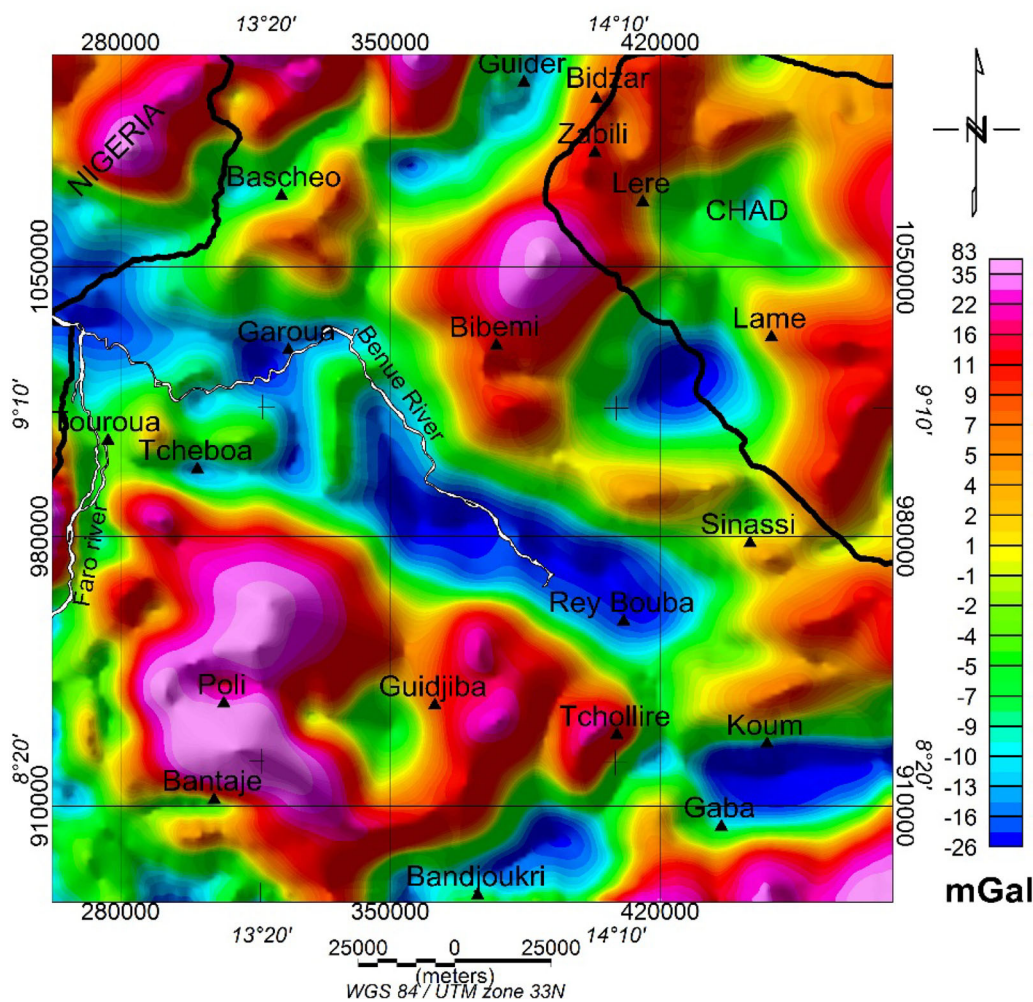


Figure 3. Free air anomaly map of the study area derived from EGM2008 gravity data.

tinental sedimentary basins (Koum, Hamakoussou, Mayo Oulo-Léré, Babouri-Figuil) are located on negative anomalies. Table 2 summarizes the correspondences between free air anomalies and regional geology.

Bouguer anomalies combine the effect of deep (regional anomaly) and shallow (residual anomaly) seated structures. In this work, we used the polynomial separation technique (Radhakrishna and Krishnamacharyulu 1990) to deduce the residual anomaly map (Fig. 7) from Bouguer anomaly map (Fig. 5). Theoretically, the selection of the adequate polynomial surface order requires good knowledge of mass distribution and large-scale geological formations of the area (Wolfgang and Smilde 2009). In this study, the fourth-order polynomial regional gravity field provides satisfactory results with respect to the known mass distribution of the area. In fact,

the fourth-order regional anomaly map of the study area (Fig. 6) exposes, in its central part, a positive anomaly trending NE-SW accordingly to the Chad-Cameroon gravity line. In addition, the residual anomaly map (Fig. 7) reflects known geological features signal: The sedimentary basins of Benue (Garoua), Koum, Hamakoussou-Mayo Oulo-Babouri-Figuil (W of Zabili) are represented by negative anomalies, while the Poli and Bibémi-Zalbi belts as well as the Sinassi granitoids are illustrated by positive anomalies (Abate Essi et al. 2017).

METHODS

Gravity investigation is an efficient tool to prospect geological structures (Eyike et al. 2010; Yushan and Yuanyuan 2017). In this paper, we used

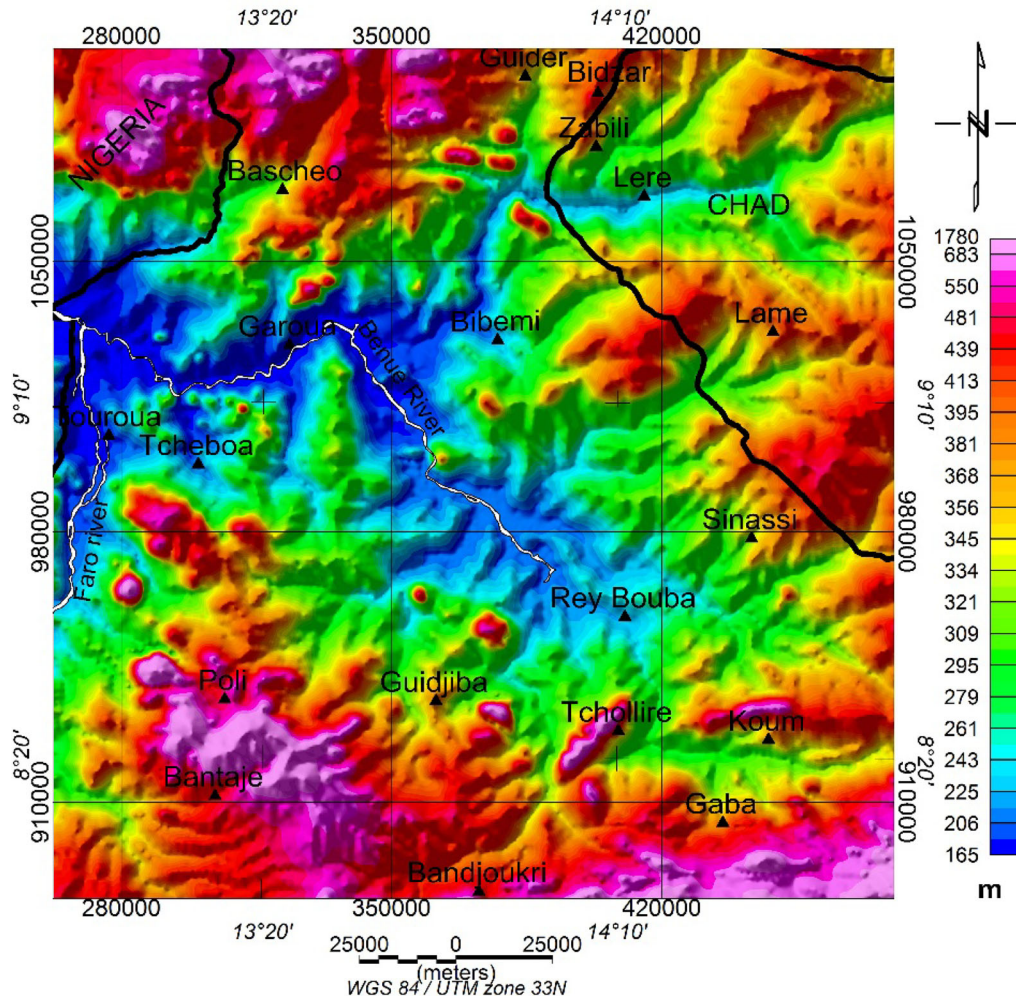


Figure 4. Topography of the study area from Etopo 1.

gravity data derived from EGM2008 to propose a model of the subsurface. The methodology involved a series of techniques that enabled to define the configuration of the basement. Depths of geological belts were estimated by radially averaged power spectrum analysis, while the disposition of structural features like faults was evaluated through Euler deconvolution.

Radially Averaged Power Spectrum Analysis

This is a quantitative technique to estimate depth based on density contrast of geological formations or terrestrial layers beneath the surface. It enables to determine Moho depth when the grid

area is large enough (Poudjom 1993; Goussi et al. 2017) and rock basement for a restricted zone (Atawa et al. 2016; Arefaee 2017). This technique applies 2D fast Fourier transform (FFT) approach on gravity data. Based on the calculated wavenumbers or frequencies, Spector and Grant (1970) showed that slopes of the log radially averaged power spectrum correspond to the depth of density discontinuity between two sources, thus:

$$h = [\Delta \log E] / [4\pi \Delta n] \tag{1}$$

where h depth, n wavelength, and E power spectrum.

The first approach of the radially averaged power spectrum (Spector and Grant 1970) was its

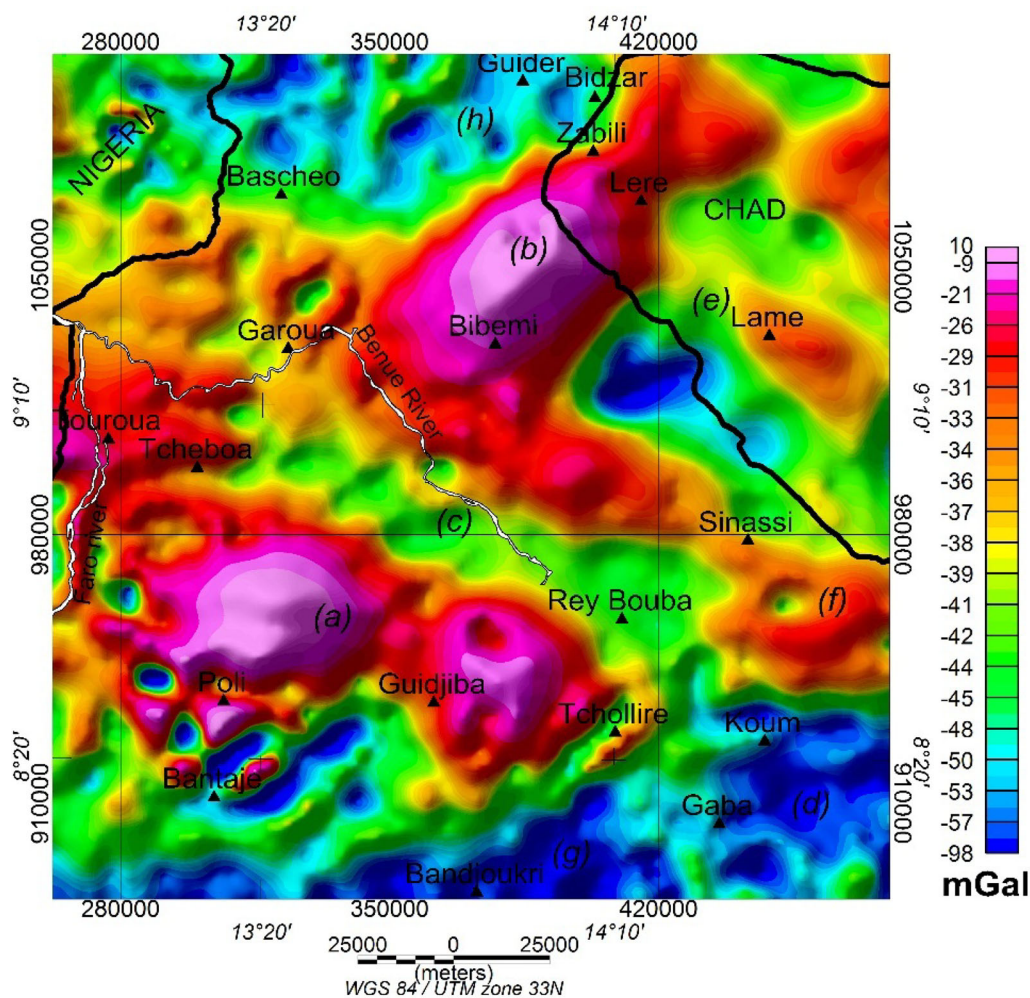


Figure 5. Bouguer anomaly map of the study area derived from EGM2008 gravity data. (a), (b), (c), (d), (e), (f), (g) and (h) are chosen anomalies for radially averaged spectrum analysis Modified from Abate Essi et al. (2017).

Table 2. Main geological formations highlighted from significant free air anomalies (Fig. 3)

Anomalies (location)	Free air anomaly (amplitude)	Geological interpretation
Garoua–Rey Bouba	Negative	Sedimentary basin of Benue Trough
Koum–Garoua	Negative	Sedimentary basin of Koum
Léré–Lamé	Negative	Sedimentary basin of Léré
SW Guider	Negative	Sedimentary basins of Hamakoussou, Mayo Oulo-Léré and Babouri-Figuil
Poli–Bantaje–Tcholliré	Positive	Volcano-sedimentary belt of Poli
Bibémi–Zabali	Positive	volcano-sedimentary belt of Bibémi-Zalbi
West of Guider	Positive	Pan-African granitoid
South of Gaba	Positive	Pan-African granitoid

application for magnetic data. Thereafter, other works enabled to implement this method to gravity data. Maus and Dimri (1995) deduced that the depth of some geological structures can be calculated

through radially averaged power spectrum technique using their density or susceptibility distributions in the Earth’s crust. Furthermore, Pawlowski (1994, 1995) demonstrated using Naidu’s formula

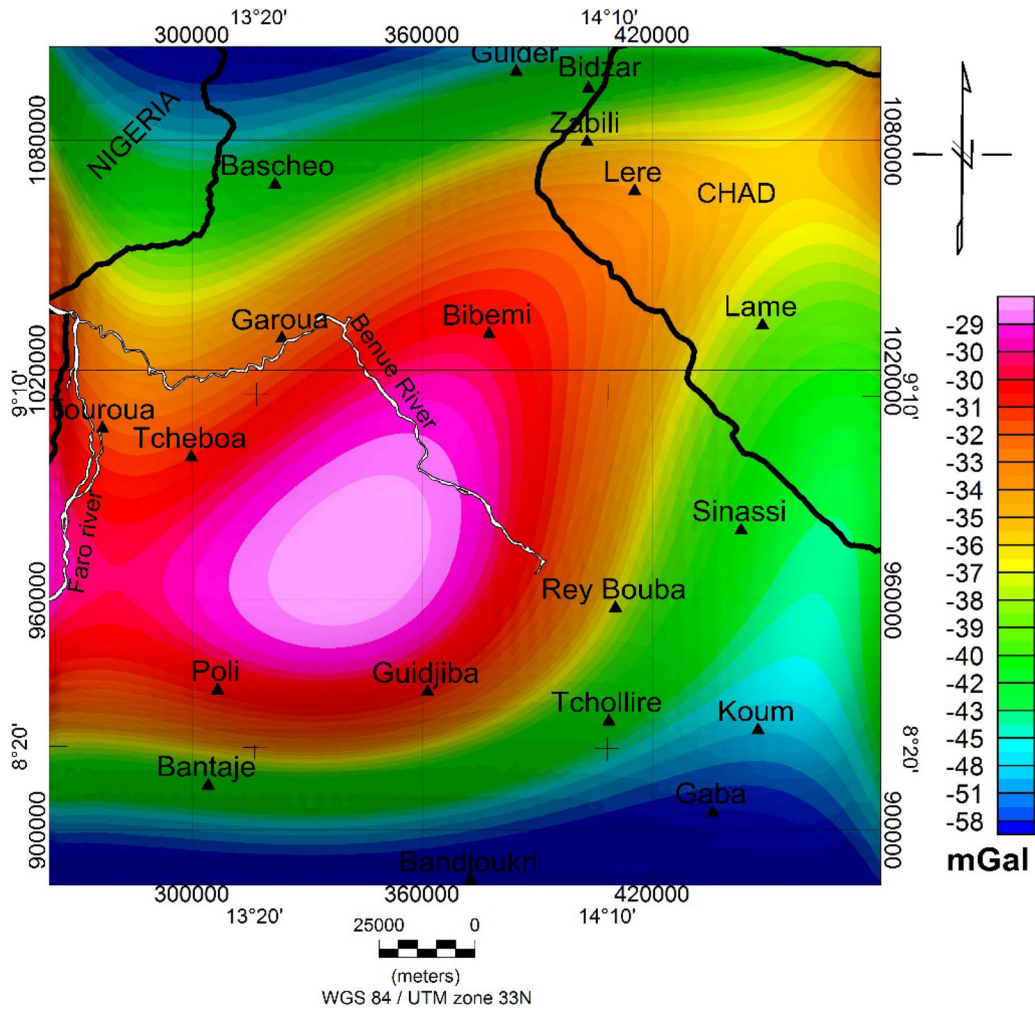


Figure 6. Regional anomaly map of the study area.

(1968) that the slope of log power spectrum of a considered density layer, which causes a gravity field, is proportional to its depth.

The first, second and third slopes represent the limit of the deepest, intermediate and shallow sources, respectively. In this paper, the computation was performed for the entire study area with $1^\circ \times 1^\circ$ grid cell to evaluate the Moho, and for some specific local anomalies to determine the basement of their sources.

Euler Deconvolution

Euler deconvolution enables to evaluate the location (position and depth) of a source responsible for gravity or magnetic field according to the degree

of homogeneity expressed as “structural index” (Thompson 1982; Reid et al. 1990). The homogeneity equation proposed by Thompson (1982) is:

$$(x - x_0)\partial g/\partial x + (y - y_0)\partial g/\partial y + (z - z_0)\partial g/\partial z = -NG \tag{2}$$

where (x_0, y_0, z_0) correspond to the coordinates of the causative source, while (x, y, z) are those of the location where gravity field (g) is evaluated; N is the structural index representing the measure of the fall-off rate of the gravity field with distance from the source, and characterizes the geometry of a particular source to be highlighted for a case study. The choice of N used to solve the homogeneity equation depends on the purpose of the study. Theoretically, N varies from 0 to 2 for gravity field. N equal to 0 is

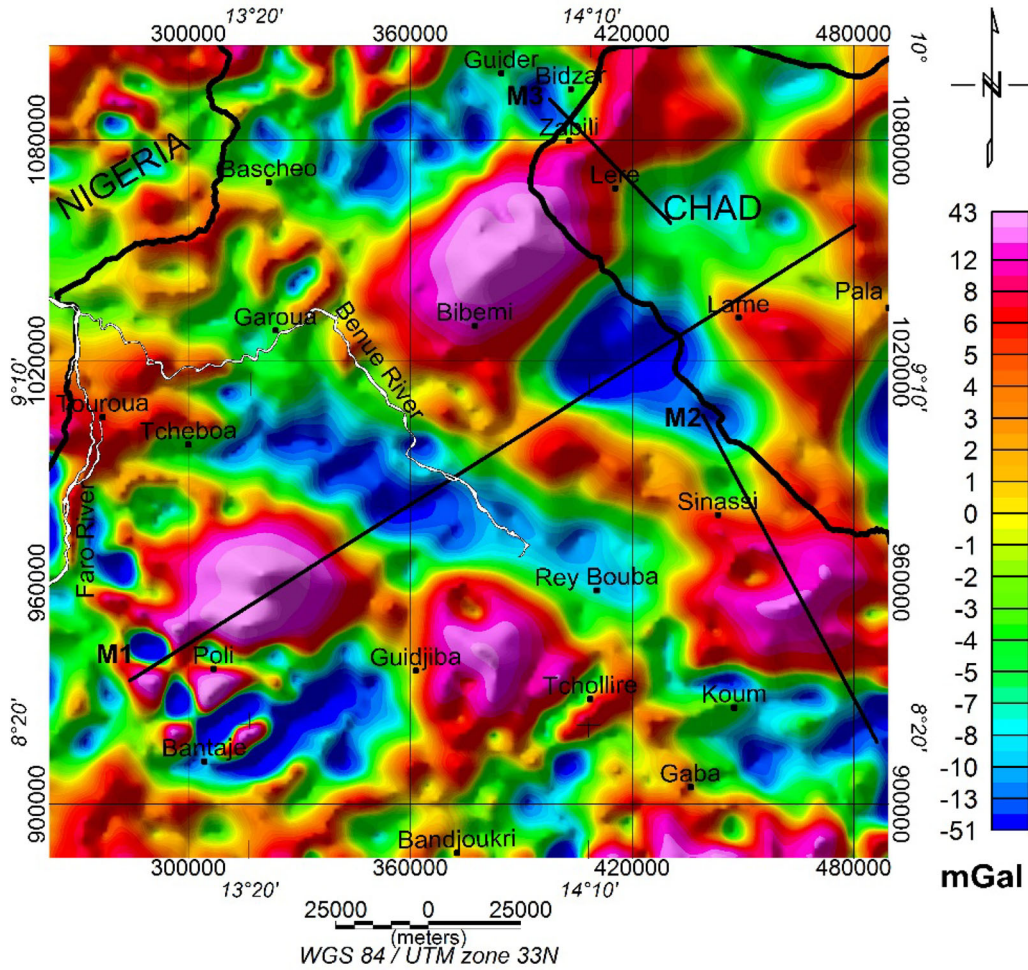


Figure 7. Residual anomaly map derived from EGM2008 gravity data. M1, M2 and M3 are profiles for gravity modeling Modified from Abate Essi et al. (2017).

an appropriate model for sill, dyke, ribbon or step structures; N equal to 1 is interesting for cylinder or pipe, and N equal to 2 is useful for sphere. A special attention is needed for $N = 0$ since this value represents the physical limit that can only be approached as the so-called infinite dimensions of the real source increase (Thompson 1982; Marcel et al. 2018a). However, Euler deconvolution is an efficient method to delineate fault or geological contact with N that comprised between 0 and 1. For this purpose, values near zero are advisable (Thompson 1982).

Maxima Horizontal Gradient Coupled to Upward Continuation

Horizontal gradient is a useful technique to delineate geological contacts or faults characterized

by the local maxima of gravity field (Philips 1998; Abate Essi et al. 2017; Marcel et al. 2018a). Upward continuation method consists of the application of a low-pass filter, which attenuates short wavelengths while amplifying high ones, highlighting the signal of deeper geological source. Thus, the combination of these two techniques enables to evaluate the contact dip of the gravity lineaments (Atawa et al. 2016; Marcel et al. 2018a). This technique consists of three main steps. Firstly, the Bouguer anomaly map is upward continued at progressive heights. Then, the horizontal gradient maxima of each upward continued map is determined. Finally, the displacement of maxima of horizontal gradient is checked to specify if the dip is vertical (superimposition of maxima) or oblique (displacement of maxima).

Gravity Modeling

Gravity modeling enables to present the relationship between the gravity field and the geological formations characterized by their densities, geometries and depths. It is a quantitative analysis of gravity field whereby a calculated curve, interpreted as the gravity response of ground model, is superimposed on the observed curve of the gravity field (Cordell 1973; Essa 2012). Crustal architecture can therefore be illustrated. For this reason, the regional geology needs to be well known as well as the tectonic events. Thus, this technique is an important tool to illustrate the underground of a mineralized zone such as the study area. In this work, the results of precedent techniques were used to constrain the different gravity bodies of models. The radially averaged power spectrum was helpful to estimate the average depths of gravity sources. Taking into account some parameters such as grid dimension of the calculated area, the slope of power spectrum vs.

wavenumbers, the results may be associated with Moho discontinuity depth, intra-crustal discontinuities or some geological formation basements. Indeed, the depths of geological belts were determined through the said technique and the shapes of gravity bodies were proposed accordingly. The residual anomaly map (Fig. 8), which exposes subsurface formation signal, was used to extract observed curves along rectilinear profiles. In addition, the estimation of Moho discontinuity depth enabled to check the crustal thickness as well as the interpretation of mantle origin rocks outcropping in the study area. Likewise, the techniques of Euler deconvolution and maxima horizontal gradient coupled to upward continuation revealed some linear structures like faults or geological contacts, and to estimate their “gravity dip” (Jaffal et al. 2010; Atawa et al. 2016; Marcel et al. 2018a). Thus, the use of the said techniques provided information for the investigation of the crustal permeability related to hydrothermal process in the study area.

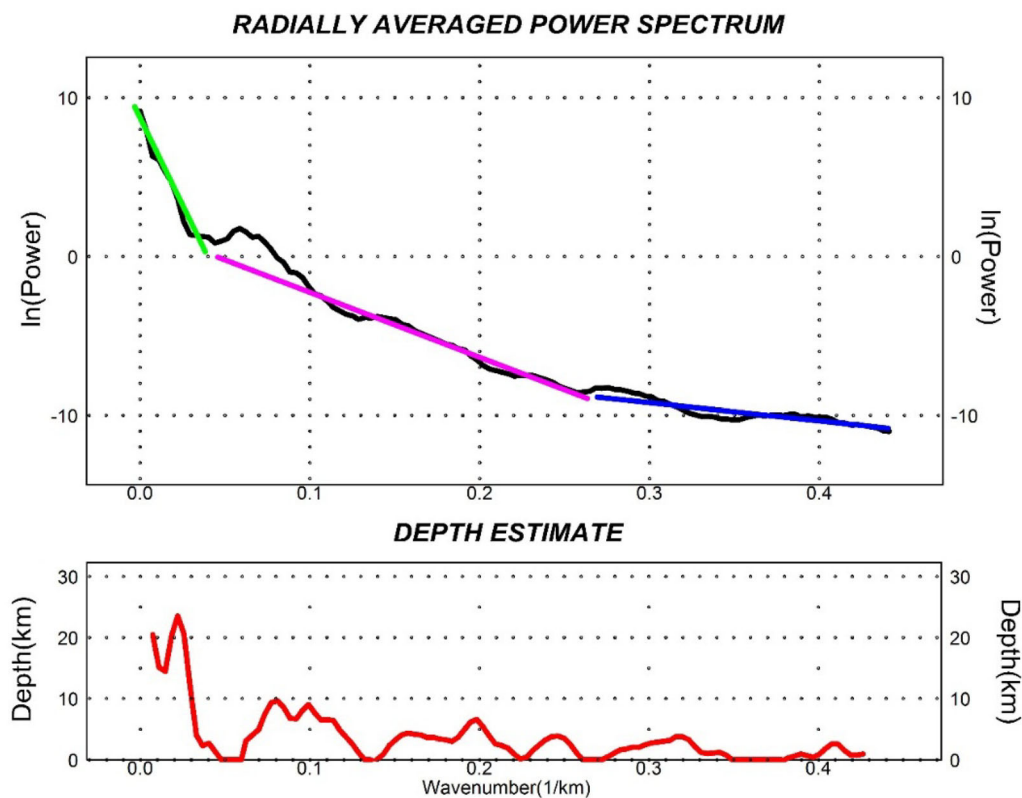


Figure 8. Radially averaged spectrum analysis of the entire study area. In the upper box, the black curve presents the power spectrum divided into three segments: deep source (green line), shallow source (purple line) and noise (blue line). The red curve in the lower box represents the estimated depth from the Spector and Grant (1970) principle.

RESULTS

Radially Averaged Power Spectrum Analysis

The Bouguer anomaly map (Fig. 5) presents some positive and negative anomalies that tally to well-known geological belts (Abate Essi et al. 2017). The radially averaged power spectrum analysis was performed to determine firstly, the Moho discontinuity depth of the entire study area, and secondly, the intra-crustal depth of density contrast inferred from some specific anomalies. The radially power spectrum was calculated by averaging the energy in all the directions for the same wavenumber. The slopes of the power spectrum curve delineate the depths of density contrasts. The energy spectrum (Figs. 8, 9) can be split into three remarkable sections comprising deep sources (green), shallow sources (purple) and noise (blue) components. Besides, the results of the computation also depend on the grid dimension. The study area, which corresponds to a $1^\circ \times 1^\circ$ (or $111 \text{ km} \times 111 \text{ km}$) grid dimension, was used for radially averaged spectrum analysis. Likewise, Poudjom (1993), Leseane et al. (2015) and Goussi et al. (2017) demonstrated the efficiency of this grid dimension to determine Moho depth. In restricted areas, this technique enables to estimate the depth of the causative source of located anomalies (Atawa et al. 2016; Arefaee 2017; Akinlalu et al. 2018). In this regard, the depths of gravity sources for the main anomalies were investigated through this technique.

Figure 8 presents the deepest discontinuity estimated in the study area at 24 km corresponding to the Moho depth. This result is in accordance with the findings of Poudjom (1993), who evaluated in the same region the crustal thickness at 25 km using terrestrial gravity data. Furthermore, Stuart et al. (1985) determined a Moho depth at 23 km using seismic data of active source, while Tokam et al. (2010) and Eloumala et al. (2014) obtained the values of 25.5 km and 25–28 km, respectively, using seismic data from passive source. Figure 9 exposes the estimated depths of gravity sources deduced from located anomalies (Table 3). Each located gravity anomaly was extracted individually for computation. The results of power spectrum analysis performed on these located anomalies enabled to investigate shallow crustal structures. The volcano-sedimentary formations characterized by positive anomalies in Poli and Bibémi areas revealed the two density contrast depths at 11.5 and 6.5 km for the

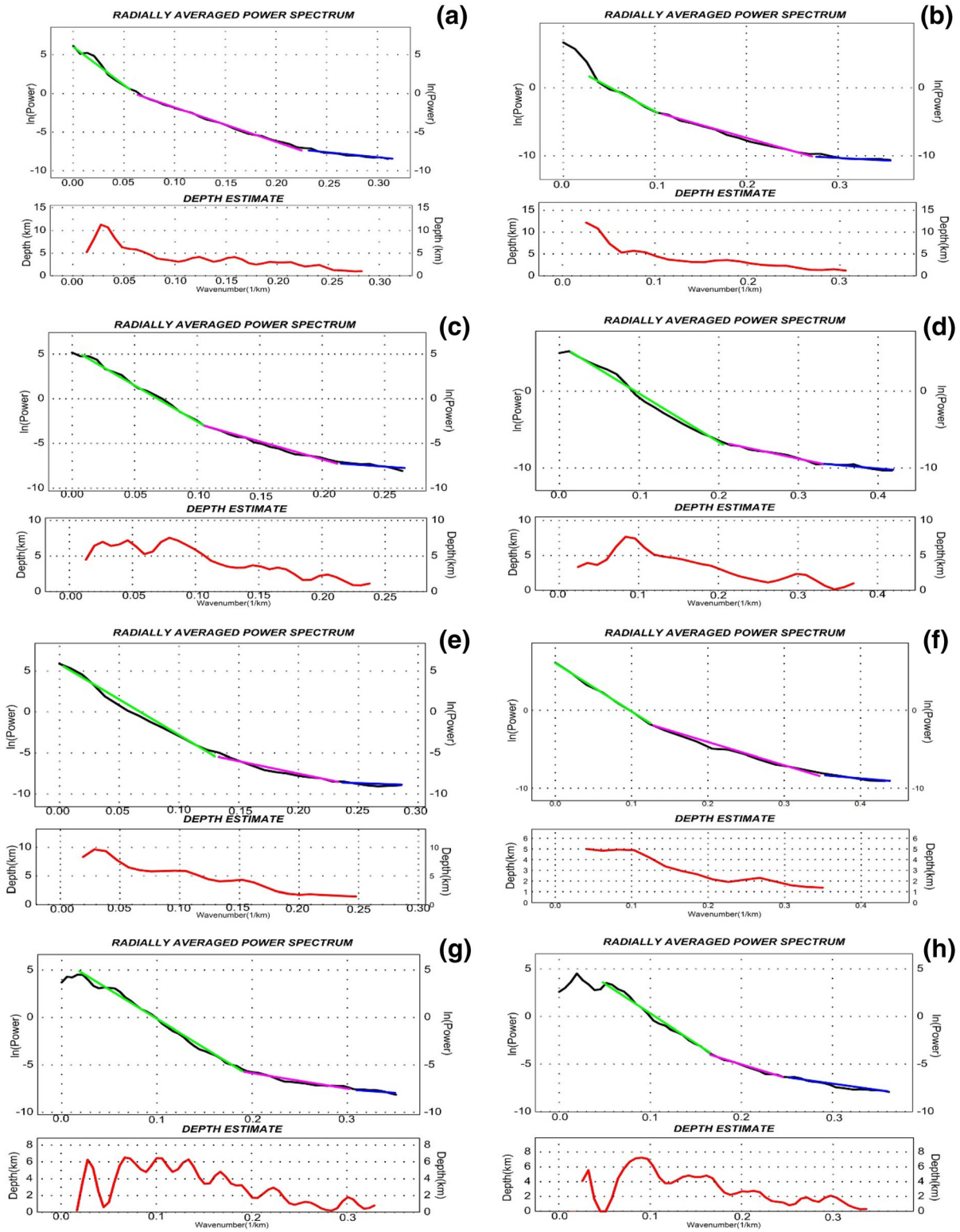
first (Fig. 9a) and 12 and 5 km for the second (Fig. 9b). The depths of causative source that were inferred from located anomalies of Sinassi, Bandjougri and Guider are 5–2 km (Fig. 9f), 6.5–4 km (Fig. 9g) and 7–4 km (Fig. 9h), respectively. The curves of radially averaged power spectrum of the negative anomalies reflecting sedimentary basins of Benue, Koum and Léré enabled to estimate the bottom of the gravity sources at 7–4 km (Fig. 9c), 7.5–5 km (Fig. 9d) and 9.5–5.5 km (Fig. 9e), respectively.

Euler Deconvolution

In the present work, a moving window of $15 \times 15 \text{ km}$ was used to solve the homogeneity equation (Thompson 1982; Reid et al. 1990) with a structural index N of 0.5. This structural index is interesting to locate structures like contacts, faults or sills. Theoretically, the perfect structural index to identify linear solution is equal to zero. However, the case of structural index equal to zero is physically impossible because it should involve a constant gravity field regardless of the distance from the source (Thompson 1982; Marcel et al. 2018a).

Figure 10 exposes the map of Euler solutions for the study area in plan (Fig. 10a) and in perspective (Fig. 10b) views. Three regions are chiefly distinguished:

- The Benue Trough characterized by very shallow lineaments. Despite the fact that some structures are identified near 10 km depth (Fig. 10b), most of the solutions were found between 0 and 5 km depth. The convexity (Fig. 10b) observed in this region may explain the weak gravity response induced by the sedimentary cover of Benue. This region is bordered by deeper structures notably in the Poli and Bibémi sectors.
- In the Poli region, along the contact with Benue Trough, a fracture extending up to 16 km depth was identified. A lineament trending E–W extending between 2 and 4 km depth was observed in the South of Bantaje locality. An alignment of NE–SW trending fractures, more or less deep, was located in Guidjiba locality. The TSZ is exposed in the Euler deconvolution map (Fig. 10a), and it extends from the south of Tcholliré until Sinassi locality, between 2 and 6 km depth.



◀ **Figure 9.** Radially averaged spectrum analysis of gravity sources deduced from located anomalies. In the upper box for each locality, the black curve presents the power spectrum divided into three segments: deep source (green line), shallow source (purple line) and noise (blue line). The red curve in the lower box for each locality represents the estimated depth from the Spector and Grant (1970) principle. The analyses were performed through the anomalies in the following localities: **a** Poli, **b** Bibémi, **c** Benue, **d** Koum **e** Léré, **f** Sinassi, **g** Bandjoukri, **h** Guider.

Table 3. Density contrast depths estimated from radially averaged power spectrum analysis (Fig. 8)

Anomalies (location)	Deep contrast obtained from the first slope (km)	Shallow density contrast obtained from the second slope (km)
Poli (a)	11.5	6.5
Bibémi (b)	12	5
Benue (c)	7	4
Koum (d)	7.5	5
Léré (e)	9.5	5.5
Sinassi (f)	5	2
Bandjoukri (g)	6.5	4
Guider (h)	7	4

Likewise, the Koum fault extends until 8 km depth.

- The region of Bibémi represents the deepest fractured zone (beneath 10 km) of the study area. This zone extends from Bibémi (Cameroon) until Zabali (Chad) following a NE-SW direction accordingly to the Poli-Ouni-anga-Kebir heavy gravity line. At the boundary of Benue Trough, Rey Bouba zone exposes deep lineament reaching 13 km depth.

Horizontal Gradient Coupled to Upward Continuation

The results of the horizontal gradient maxima coupled with upward continuation are presented in Figure 11. Linear discontinuities can be observed as well as their dip. These structural discontinuities are usually interpreted as faults or geological contacts (Jaffal et al. 2010; Atawa et al. 2016; Marcel et al. 2018a). It is therefore possible to evaluate the “gravity dip” of some geological structures from

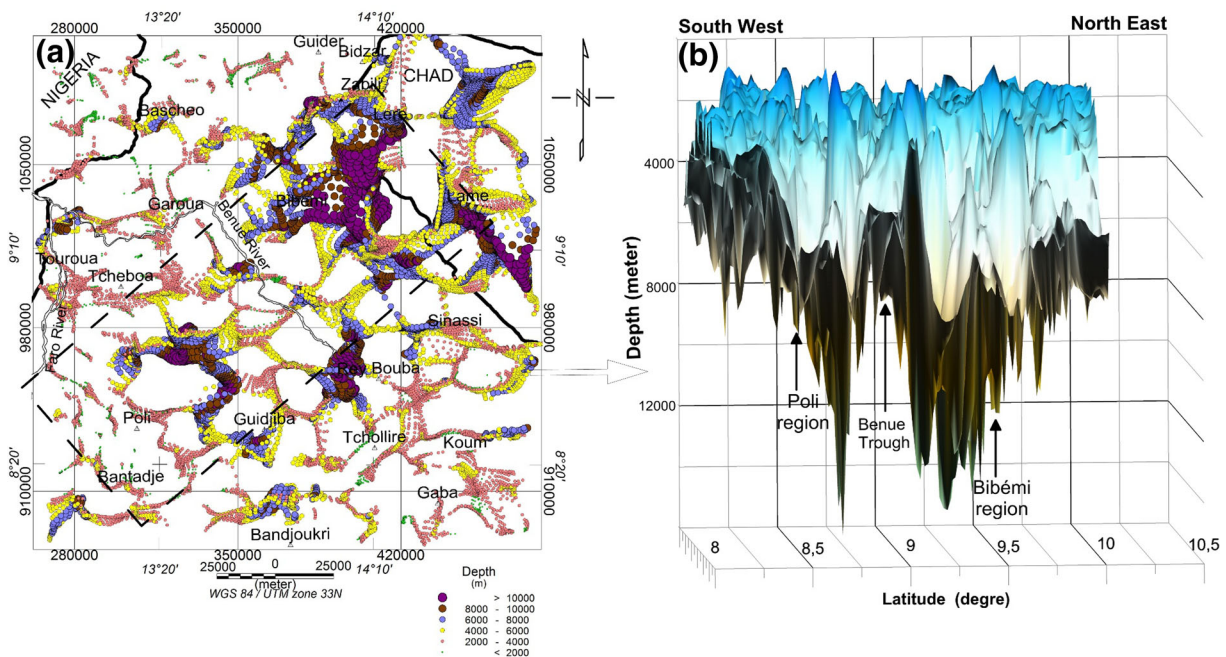


Figure 10. Euler deconvolution map of the study area in plan (a) and perspective (b) views. According to the gravity potential field, the plan view (a) exposes the distribution of the Euler solutions in the study area, whereas the perspective view (b) reveals the depth extension of fractures in the NE-SW direction.

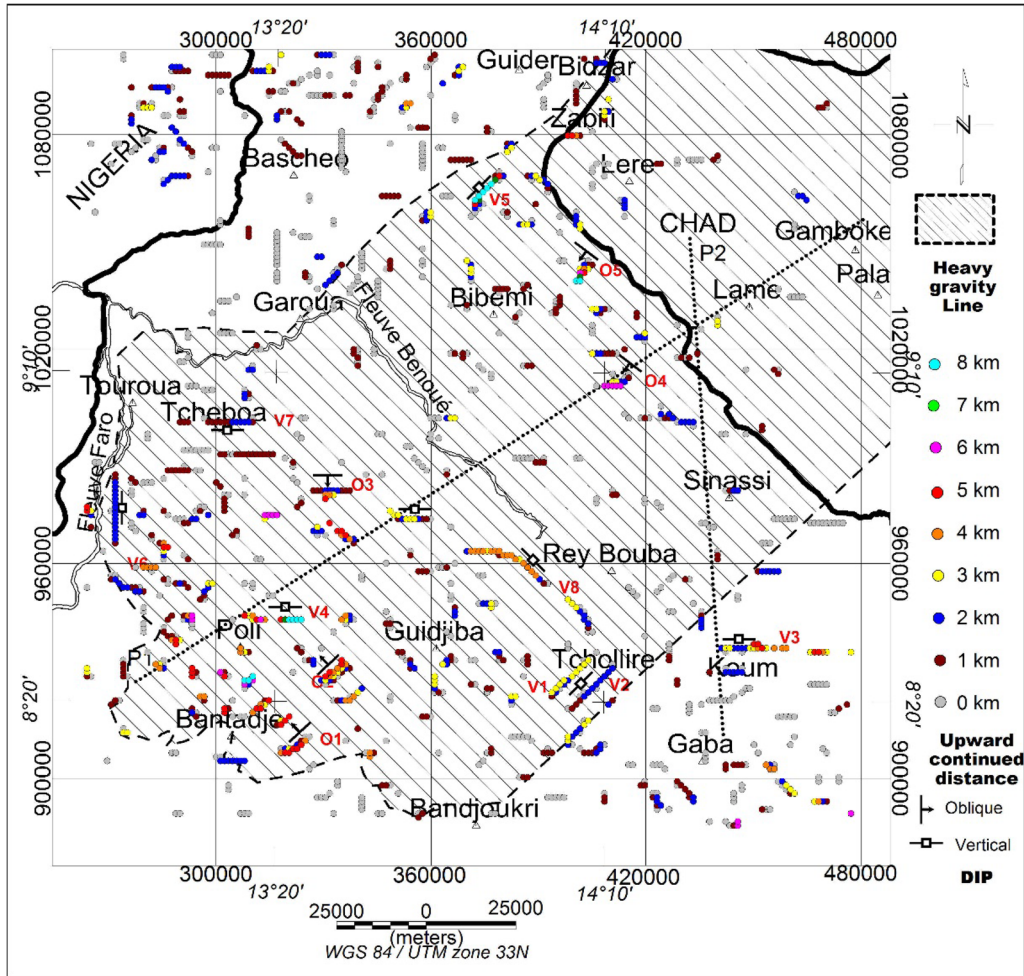


Figure 11. Superposition of horizontal gradient maxima coupled with upward continuation. P1 and P2 are profiles for synthetic crustal models.

gravity data. In the study area, we applied a progressive and regular upward continued distance of 1 km until a maximum height of 8 km. Lineament dips were visible at the SW and NE sides of the Benue Trough illustrating its limits. However, the Benue Trough exposes few structural features because Cretaceous sedimentary cover obliterates the gravity signal of basement. Some lineaments derived from maxima of upward continuation at 0 km are individual, without superimposition of adjacent lineaments at progressive heights. These lineaments are very superficial and may be assimilated to noise or shallow features such as weathered rocks or soil (Wolfgang and Smilde 2009; Goussi et al. 2017).

Vertical dips were characterized by the superposition of horizontal gradient maxima at different upward distances. Figure 11 brings out the following vertical lineaments.

- Two parallel lineaments (V1 and V2) trending NE–SW identified around Tcholliré locality;
- Koum fault (V3) trending E–W;
- E–W Balché fault (V4) located at the north of Poli;
- At the north of Bibémi, a lineament (V5) trending NE–SW;
- N–S fault (V6), which appears around Faro river;

- Vertical lineaments at edge of Benue Trough, located especially in Tcheboa (V7) with E–W direction, and at the west side of Rey Bouba (V8) oriented NW–SE.

Oblique dip involves the displacement of horizontal gradient maxima gradually with increasing upward continued distances. In the study area, five main lineaments were identified, namely:

- Two lineaments (O1 and O2) located at the E and NE of Bantajé localities. Both structures follow NE–SW orientation and dip toward NW;
- At SE of Tcheboa locality, the lineament O3 is oriented E–W and dips toward the S;
- Two lineaments O4 and O5 trending NW–SE and dipping toward SW located at the NE and SW of Bibémi.

Gravity Modeling

Gravity modeling proposes a structure of the upper part of the crust that may explain the observed gravity anomalies, inferred from density contrast of geological bodies. The solution models that interpret a specific potential field are not unique (Blakely 1996; Jones-Cecil 1995; Arefae 2017). A good knowledge of the geology and previous geophysical works on the study area are required. In our case, some information on the basement was obtained through spectral analysis technique, which evaluates the main density contrasts of geological formations. The modeling method interactively superimposes the observed gravity anomaly curve and the calculated or generated anomaly curve inferred from densities characterized bodies within the crust. It implies to build in the crust some geological bodies that are defined by density and polygonal cross sections with finite extensional length in the

strike direction (Rasmussen and Pedersen 1979; Yashan and Yuayan 2017). A change of bodies' parameters (density, depth, shape) will automatically modify the calculated curve. The best model presents a calculated anomaly curve that fits very well the observed anomaly curve and proposes a coherent underground structure. For this purpose, residual anomaly map translates the influence on the lithology of the superficial part of the earth. The modeling program used in this study was the GM-SYS established by NGA (2004). This program is based on the algorithms of Won and Bevis (1987), which are incorporated the formulations from Rasmussen and Pedersen (1979). The residual anomaly map (Fig. 7) was used to propose three models (M1, M2 and M3) because it exposes the variation of gravity anomaly of the upper part of the terrestrial crust. These models were built using known geological information of the study area and considering a granito-gneiss basement that was intruded and covered by various lithologies. The density and density contrasts of gravity bodies are presented in Table 4.

The model M1 (Fig. 12) is proposed for a 245-km-long profile trending NE–SW, which links the localities of Poli (Cameroon) and Pala (Chad). It crosscuts negative anomalies of the Benue Trough and covers positive anomalies inferred from high-density rocks of the volcano-sedimentary formations of the Poli and Bibémi-Zabili belts. The overall Poli belt is characterized by positive anomaly with some variations of amplitude where sedimentary and volcanic formations crop out. Toteu et al. (2006) described conglomerate layers in the sedimentary sequences, whereas Angoua et al. (2008) brought out alluvia and sandstone, especially in the Balché, Nigba and Noukla areas. The sedimentary formations are marked by low density, namely 2.5 g cm^{-3} (Telford et al. 1990), responsible for the negative anomalies. On the other hand, volcanic rocks consisting of tholeiitic basalt, tuffs, sodic rhyolites and trachytes (Toteu et al. 2006; Angoua et al. 2008)

Table 4. Densities of geological bodies used for modeling Adapted from Telford et al. (1990)

Materials		Density contrast of rocks
Intrusive	Enclosing	
Mafic igneous rock (2.79 g cm^{-3})	Granite–gneissic basement (2.67 g cm^{-3})	+ 0.12
Sedimentary rock (2.50 g cm^{-3})	Granite–gneissic basement (2.67 g cm^{-3})	– 0.17
Lava (2.90 g cm^{-3})	Granite–gneissic basement (2.67 g cm^{-3})	+ 0.23

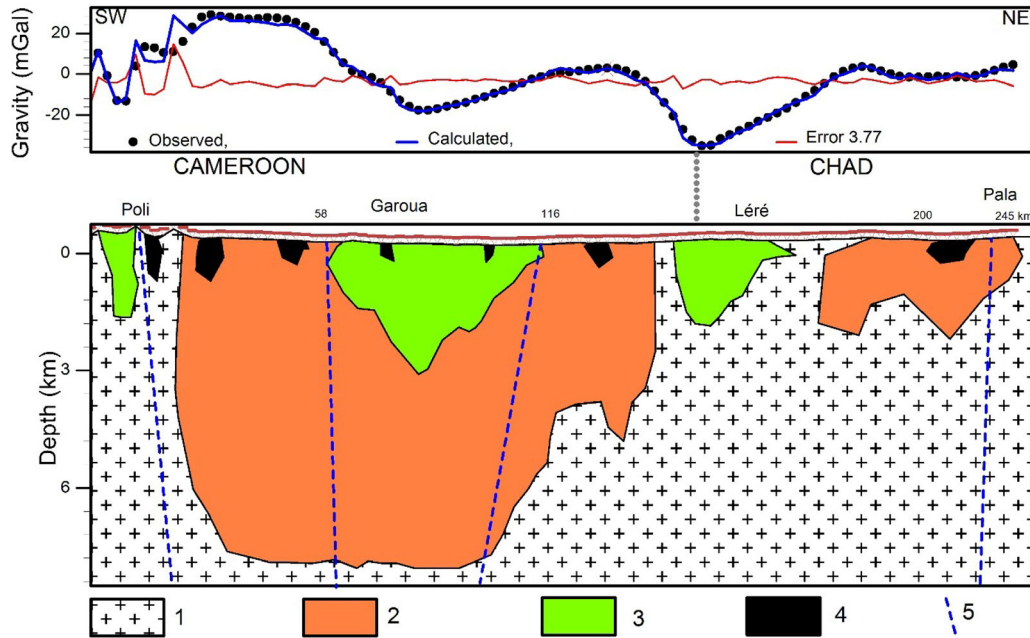


Figure 12. Gravity model from profile M1. 1: granito-gneiss basement (density = 2.67 g cm^{-3}) 2: volcano-sedimentary formations (density = 2.79 g cm^{-3}) 3: sedimentary basin (density = 2.5 g cm^{-3}) 4: volcanic lavas (density = 2.9 g cm^{-3}) 5: major fault.

have greater density. The volcano-sedimentary belts of Poli (Cameroon) and Bibémi-Zabili (Chad) are unique (Njel 1986; Penaye et al. 2006; Bouyo et al. 2015a). The model M1 presents these volcano-sedimentary belts covered, in its center part, by low-density sedimentary formations of Benue Trough represented mainly by cretaceous sandstones. Previous works (Njel 1986; Pinna et al. 1994; Abate Essi et al. 2017) demonstrated that the Yola–Garoua branch of Benue Trough covers the volcano-sedimentary formations of the Poli and Bibémi-Zalbi belts. Mafic igneous rocks belonging to this volcano-sedimentary belt are characterized by moderate density of 2.79 g cm^{-3} . Greenstone belts (Isseini 2011; Bouyo et al. 2015b; Mbaguedje 2015) are distinguished around volcano-sedimentary formations in the NW Cameroon and Mayo Kebbi (Chad) domains. Cenozoic volcanic formations are also exposed within the Garoua basin. These are basaltic, phonolitic, trachytic rhyolitic formations belonging to the Cameroon Volcanic Line (Ngounouno et al. 1997). The said formations are associated with a granite–gneissic basement that are characterized by a crustal density of 2.67 g cm^{-3} . The model illustrates the continuity of volcano-sedimentary belt on the heavy gravity line along the Benue Trough until Mayo Kebbi in Chad. The end of the model presents

the granitoids of Pala (Chad) and mafic igneous formations described by Pouclet et al. (2006).

The model M2 (Fig. 13) follows a NW–SE profile extending along 100 km distance. On the profile, positive anomaly is bordered by low-magnitude anomalies. In the Sinassi region, the spectral analysis highlighted a density contrast discontinuity at 5 km depth, which corresponds to the limit depth of the mafic igneous rocks of the volcano-sedimentary belt. Louis (1970) suggested the appellation “heavy line” for the Chad–Cameroon gravity line trending NE–SW because of the presence of high-density rocks. In this sector, Bouyo et al. (2015b) described metavolcanic rocks associated with greenstones, which differ from transitional to calc-alkaline magma compositions with mostly high Mg concentration. These mafic rocks should be responsible for this positive gravity anomaly. Finally, the low-density sedimentary basins of Koum and Léré consisting mainly of sandstones, clay and conglomerates (Nolla et al. 2015) border the model. The model brings out the two litho-structural units namely the North and Adamawa domains (Toteu et al. 2001, Van Schmus et al. 2008) related to the Koum fault and TSZ. The basement consists manifestly of granitoids and low-to-high-grade gneiss (Diab 2016).

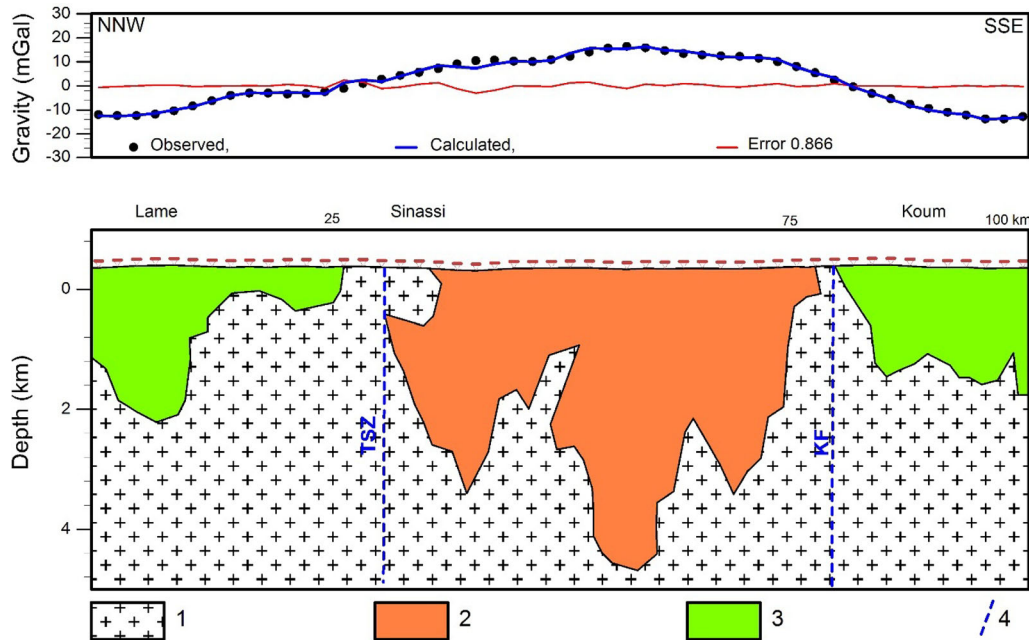


Figure 13. Gravity model from profile M2. 1: granito-gneiss basement (density = 2.67 g cm^{-3}) 2: volcano-sedimentary formations (density = 2.79 g cm^{-3}) 3: sedimentary basin (density = 2.5 g cm^{-3}) 4: major fault TSZ: Tcholliré shear zone KF: Koum fault.

The third model M3 (Fig. 14) pertains to a profile of 47 km according to a NW–SE direction. The model starts by the intra-continental basin of Babouri-Figuil, which is mostly filled by low-density sandstones associated with silt, maltstone and limestone (Schwoerer 1962). The end of the profile is marked by the Chadian sedimentary basin of Léré with low-density components involving low-magnitude gravity anomaly at the Mayo Kebbi domain. The granite–gneissic basement presents some intrusions of denser materials influencing the ascent of the curve. The mafic to intermediate complex and the greenstone belt are presented in the model as mafic igneous rocks within the basement. The granitoid batholith of this geological domain is integrated in the basement.

DISCUSSION

The geology of north-central Cameroon involves two main litho-structural domains of Cameroon (Toteu et al. 2001; Van Schmus et al. 2008) separated by the sinistral TSZ and characterized by various geological formations. Louis (1970) defined an alignment of positive gravity anomalies trending NE–SW known as the Poli–Ounianga–Kebir heavy

line. Along this Chado-Cameroonian gravity axis, interesting uraniferous and auriferous deposits are found on the southwestern to the northeastern sides of the Benue Trough (Kusnir and Moutaye 1997; Tchameni et al. 2013; Mbaguedje 2015; Abate Essi et al. 2017). Gravity modeling of the subsurface was performed to show the coherent relationship between geological formations, mineral deposits and gravity signal. In this regard, gravity data derived from the EGM2008 geopotential field model, which consists of terrestrial, marine and satellite data, are suitable for gravity investigation (Eyike et al. 2010; Abate Essi et al. 2017; Marcel et al. 2018a, b). The various techniques used enable to recognize some patterns of the terrestrial crust.

The radially averaged power spectrum analysis (Spector and Grant, 1970) showed a mean depth of source at 24 km in the study area that can be associated with the Moho discontinuity and enabled to identify density contrast depths around some specific gravity anomalies. These results are in accordance with the assumption of a thinned crust in the area (Stuart et al. 1985; Poudjom 1993; Tokam et al. 2010; Fishwick and Bastow 2011; Eloumala et al. 2014). This thinned crust has been interpreted as a beginning of rifting in the Adamawa Massif (Poudjom 1993) and in the Upper Benue Trough (Benkhelil

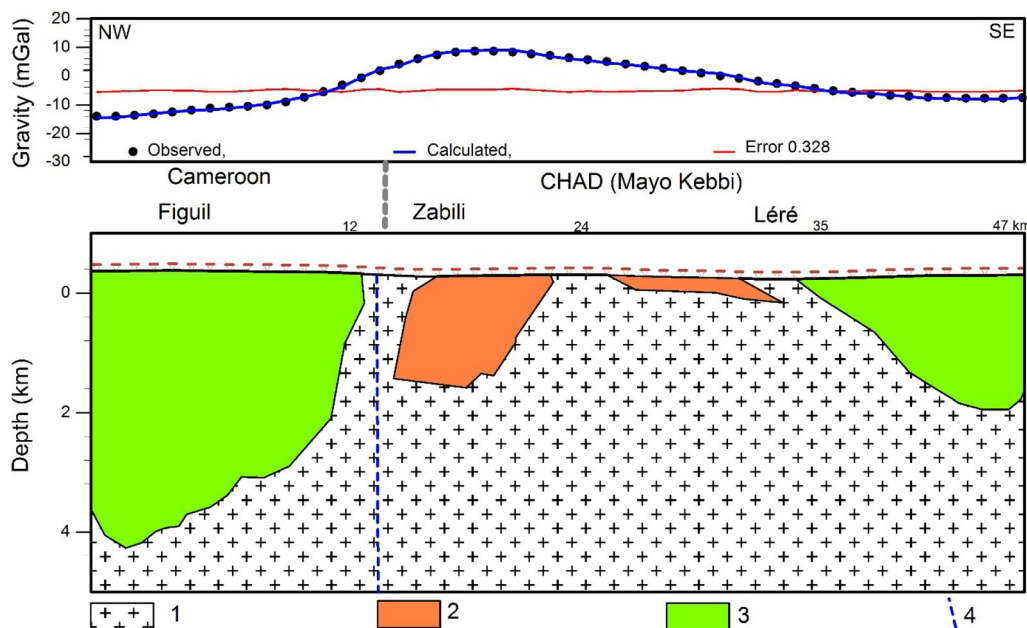


Figure 14. Gravity model from profile M3. 1: granito-gneiss basement (density = 2.67 g cm^{-3}) 2: volcano-sedimentary formations (density = 2.79 g cm^{-3}) 3: sedimentary basin (density = 2.5 g cm^{-3}) 4: major fault.

1986). The proximity of the high-density upper mantle to the surface in the study area raises many implications. In the Pan-African Orogenic Belt, the presence of several ultramafic to mafic rock suggests the importance of mantle–crust interaction (Toteu et al. 2004) and the intrusion of mantellic materials into the crust (Mbagedje 2015). Barbarin (1998) illustrated the relation between granitoid types, their origins and their geodynamic environments. Thus, the granitoids registered in the study area have mantle and mixed crustal-mantle origins. The calc-alkaline granitoids of the Poli, Bibémi belts and the Mayo Kebbi batholith (Njel 1986; Pouclet et al. 2006; Tchameni et al. 2013; Bouyo et al. 2015b) derived obviously from a mixed crustal-mantle source. In addition, (Dawai et al. 2013) pointed out the mantle signature of the Guider alkaline syenite. Actually, the ultramafic and mafic rocks are characterized by higher density than the silicic granitoids or detrital sedimentary rocks (Table 4).

The solutions of Euler deconvolution and horizontal gradient maxima coupled to upward continuation technique brought out lineaments interpreted as fractures or faults. The Cretaceous Benue Trough made of low-density sediments highlights very few lineaments. In return, the filtering of the geopotential field presented its neighboring formations,

namely Poli and Bibémi-Zalbi belts, as fractured zones marked by the deepest faults of the study area. These crustal fractures put in evidence the perviousness of the upper part of the Earth. Likewise, the three models took into account the density of the main geological belts that interpret graphically the gravity anomalies. The geometry of geological bodies was in adequacy with the density contrast depth in the study area. Besides, more or less dense materials were brought out beneath the Benue Trough as well as in the Poli, Bibémi and Sinassi regions. Consequently, the name “heavy” gravity line in the study area can be manifestly considered as a set of more or less dense geological materials in the upper crust following NE–SW direction. Gold deposits line up on this gravity line, especially around the TSZ (Abate Essi et al. 2017). Auriferous quartz veins studied in this area present the analogous direction interpreted as regional strike slip shear zones trending NE–SW, similar to the TSZ (Tchameni et al. 2013). Thus, fractures highlighted in this work brought out the crustal permeability in the study area illustrating migratory passages for mantle formations found at the surface. Besides, these fractures zone are favorable for hydrothermal and Au–U-mineralized fluids migration.

Finally, two synthetic models of the geological basement (Figs. 15, 16) are proposed to illustrate the 2D geometry of the mineralized crust of the study area including the Poli and Rey Bouba orogenic belts. These synthetic models take into account the main results of this study and the known geological information of the region. The subsurface of the models is more detailed than the deepest part and is

deduced from the power spectrum analysis of the located anomalies, the technique of Euler deconvolution and maxima horizontal gradient coupled to upward continuation and gravity modeling. This is justified because the external part of the crust is evidently most well known. Moho discontinuity depth is the main information obtained that describes the deepest part of the study area and

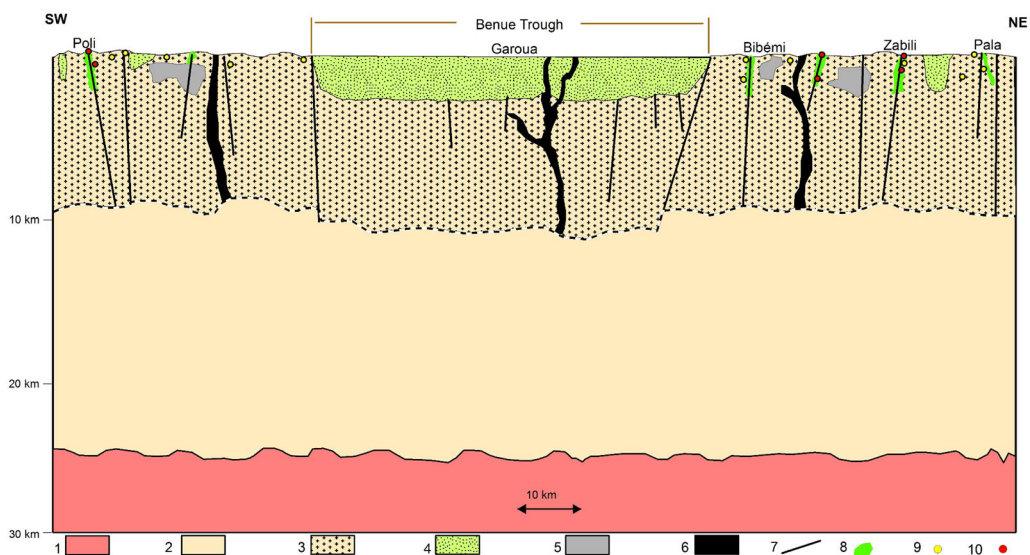


Figure 15. Synthetic model of the crust around the Benue Through. 1 Upper mantle, 2 crust, 3 Neoproterozoic granite-gneiss basement, 4 Cretaceous sandstone, 5 mafic to ultramafic rocks, 6 Cenozoic volcanic rocks, 7 faults, 8 hydrothermal fluid, 9 gold, 10 uranium.

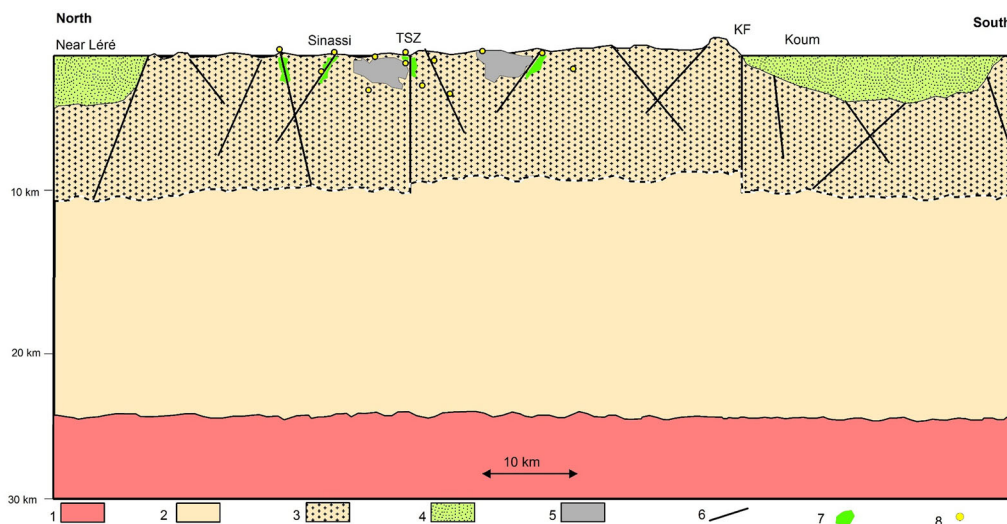


Figure 16. Synthetic model of the crust around the Tcholliré SZ. TSZ: Tcholliré SZ, KF: Koum fault. 1 Upper mantle, 2 crust, 3 Neoproterozoic granite-gneiss basement, 4 Cretaceous sandstone, 5 high-density Fe-Mg-enriched rocks, 6 faults, 7 hydrothermal fluid, 8 gold.

establishes the mantle origin of some rocks outcropping in the study area. The filtering of gravity field revealed that the Poli, Bibémi and Sinassi regions coincide with both positive gravity anomalies (Figs. 5, 7) and deep fractures zones (Fig. 10) superimposing ore deposit sectors (Fig. 2). Hydrothermal fluid migration and fractures seem to be the key factors that influence gold and uranium mineralization in the study area (Kouske et al. 2012; Mbagedje 2015; Abate Essi et al. 2017).

The synthetic model of the crust around the Benue Trough (Fig. 15) is proposed for a profile trending NE–SW (Fig. 11) and incorporates the main findings of this work. The filtering of gravity data highlighted faults, high-to-low-density geological bodies. Uranium occurrence in Kitongo near Poli and in Zabili (Fig. 2) is related to albitization and metasomatic processes along faults and fractured areas within granitic formations (Oesterlen and Vetter 1986; Kouske et al. 2012; Mbagedje 2015). Fractures and faults control fluid circulation and mineralization of uranium. Heat transfer and hydrothermal fluid circulation were derived from magma emplacement of the batholith (Eldursi et al. 2009). Likewise, magmatism played a role in the dynamics of the mineralizing fluids during gold mineralization within the heavy gravity line (Tchameni et al. 2013; Abate Essi et al. 2017). Lerouge et al. (2000) demonstrated similarly in the French Massif Central that the compositions of the mineralizing fluids as well as the control of fluid regime evolve with the successive depositions of gold. Patterns obtained from filtering of potential field enabled to analyze the relation between potential field and spatial distribution of ore deposits (Faure et al. 2009). The model also shows volcanic formations around the Poli (Njel, 1986), Garoua (Ngounouno et al. 1997) and Bibémi (Isseini 2011; Mbagedje 2015) zones.

The second synthetic model of the crust around Sinassi (Fig. 16) pertains to a N–S profile between the intra-continental sedimentary basin of Léré and Koum. As the previous model, Figure 16 presents the TSZ as the major tectonic feature of this region. This shear zone is interpreted as the southeastern edge of the Poli–Ounianga–Kebir gravity line hosting auriferous deposits (Abate Essi et al. 2017). Neoproterozoic granitoids and greenstones carrying gold deposits are located nearby the TSZ (Laplaine 1968; Toteu et al. 2008). This shear zone, which was also highlighted by the geophysical results, influenced hydrothermal fluids responsible for gold-

mineralized lodes described in the region (Toteu et al. 2008; Tchameni et al. 2013). Thus, primary gold deposits with associated metals like Cu, Ag and Ni as well as alluvial gold (Pinna et al. 1989) are the result of the migration of mineralized fluid (Kusnir and Moutaye 1997; Bierlein et al. 2006; Rabeau 2009).

CONCLUSION

The gravity data derived from EGM2008 enabled us to model the geological basement of the north-central Cameroon. The gravity model shows the geological architecture that may explain the auriferous and uraniferous ore deposits found along the Poli–Ounianga–Kebir heavy line. The calculated Moho discontinuity depth is in accordance with previous geophysical works. Furthermore, the filtering revealed the most fractured zones around the Poli and Bibémi regions, which may be propitious to the presence of hydrothermal fluid responsible for uranium mineralization found in these regions. Similarly, gold deposits described in the study area should follow the same mineral formation. This case study points out the crustal permeability for mineral deposits, especially gold and uranium in the Central African Fold Belt. Besides, this study highlighted high-density geological formations inside the crust justifying the mafic to ultramafic rocks and calc-alkaline to alkaline granitoid outcropping in the study area. The targets for detailed mineral exploration are defined on positive gravity anomaly chiefly around the Poli, Bibémi, Sinassi and in Pala regions.

REFERENCES

- Abate Essi, J. M., Marcel, J., Yene Atangana, J. Q., Diab, A. D., Fita, D. E., Mbossi, E. F., et al. (2017). Interpretation of gravity data derived from the Earth Gravitational Model EGM2008 in the Center-North Cameroon: Structural and mining implications. *Arabian Journal of Geosciences*, 10, 130–132. <https://doi.org/10.1007/s12517-017-2919-y>.
- Akinlalu, A. A., Adelusi, A. O., Olayanju, K. A. N., Adiat, G. M., Omosuyi, G. O., Anifowose, A. Y. B., et al. (2018). Aeromagnetic mapping of basement structures and mineralisation characterisation of Ilesa Schist Belt, Southwestern Nigeria. *Journal of African Earth Sciences*, 138(2018), 383–391.
- Amante, C., & Eakins, B. W. (2008). ETOPO1 1arc-minute global relief model: Procedures, data sources and analysis. *NOAA Technical Memorandum*. NESDIS NGDC-24.

- Angoua, B. S. E., Bassahak, J., Béa, A. B., Hell, J. V., Kambou, R., Ngako, V., et al. (2008). Geological map of Cameroon, Poli Sheet NC -33-II. Center for Geological and Mining Research of Garoua, Ed. GEOS.
- Arefaee, H. A. (2017). Crustal modeling of the central part of the Northern Western Desert, Egypt using gravity data. *Journal of African Earth Sciences*, 2017, 248–263.
- Atawa, M., Zouaghi, T., & Souei, A. (2016). Gravity constraints on the underground structural framework and associated volcanism of the Maghrebic allochthonous domain: The Sejene Numidian flysch, Tunisian Tell. *Journal of African Earth Sciences*, 116, 248–263. <https://doi.org/10.1016/j.jafrearsci.2016.01.008>.
- Barbarin, B. (1998). A review of the relationships between granitoid types, their origins and their geodynamic environments. *Lithos*, 46, 605–626.
- Benkheilil, J. (1986). Structure and geodynamics evolution of the intracontinental Benue-Trough (Nigeria). Thesis, University of Nice, Pub Elf (Nigeria) Ltd. 202 p.
- Bierlein, F. P., Murphy, F. C., Weinberg, R. F., & Lees, T. (2006). Distribution of orogenic gold deposits in relation to fault zones and gravity gradients: Targeting tools applied to the Eastern Goldfields, Yilgarn Craton, Western Australia. *Miner Deposita*, 2005, 1–20. <https://doi.org/10.1007/s00126-005-0044-4>.
- Blakely, R. J. (1996). *Potential theory in gravity and magnetic applications*, 1980. Bose, MK: Cambridge University Press.
- Bouyo, H. M., Penaye, J., Njel, U. O., Moussango, A. P. I., Sep, N. J. P., Nyama, A. B., et al. (2015a). Geochronological, geochemical and mineralogical constraints of emplacement depth of TTG suite from the Sinassi Batholith in the Central African Fold Belt (CAFB) of northern Cameroon: Implications for tectonomagmatic evolution. *Journal of African Earth Sciences*, 116, 9–41. <https://doi.org/10.1016/j.jafrearsci.2015.12.005>.
- Bouyo, H. M., Zhao, Y., Penaye, J., Zhang, S. H., & Njel, U. O. (2015b). Neoproterozoic subduction-related metavolcanic and metasedimentary rocks from the Rey Bouba Greenstone Belt of north-central Cameroon in the Central African Fold Belt: New insights into a continental arc geodynamic setting. *Precambrian Research*, 261(2015), 40–53. <https://doi.org/10.1016/j.precamres.2015.01.012>.
- Caby, R. (1989). Precambrian terranes of Benin, Nigeria and Northeast Brazil and the late Proterozoic South Atlantic fit. *Geological Society of America Special Paper*, 230, 145–158.
- Chicharro, E., Martín-Crespo, T., Gómez-Ortiz, D., López-García, J. A., Oyarzun, R., & Villaseca, C. (2015). Geology and gravity modeling of the Logrosán Sn–(W) ore deposits (Central Iberian Zone, Spain). *Ore Geology Reviews*, 65, 294–307. <https://doi.org/10.1016/j.oregeorev.2014.10.005>.
- Collignon, L. (1968). Gravimétrie de reconnaissance de la République Fédérale du Cameroun. *O.R.S.T.O.M.* (Paris).
- Collignon, L. (1969). Contribution géophysique à l'étude du bassin de la Bénoué. *O.R.S.T.O.M.* (Paris).
- Cordell, L. (1973). Gravity analysis using an exponential density depth function-San Jacinto Graben, California. *Geophysics*, 38(4), 684–690.
- Dawai, D. (2014). Les plutons de Guider et de Bossoum-Pologozom (chaîne panafricaine au Nord-Cameroun): Analyse pétrographique, structurale, magnétique, géochronologique et implications géodynamiques. Thèse de Doctorat de l'Université de Toulouse-France en cotutelle avec l'Université de Ngaoundéré-Cameroun.
- Dawai, D., Bouchez, J. L., Paquette, J. L., & Tchameni, R. (2013). The Pan-African quartz syenite of guider (north-Cameroun): Magnetic fabric and U-Pb dating of a late orogenic emplacement. *Precambrian Research*, 236, 132–144. <https://doi.org/10.1016/j.precamres.2013.07.008>.
- Diab, D. A. (2016). Apport de la gravimétrie à la connaissance de la région du Ouaddai (Est du Tchad). Thèse Doctorat de l'Université de Yaoundé 1 (Cameroun).
- Eldursi, K., Branquet, Y., Guillou-Frottier, L., & Marcoux, E. (2009). Numerical investigation of transient hydrothermal processes around intrusions: Heat-transfer and fluid-circulation controlled linearization patterns. *Earth & Planetary Science Letters*, 208(2009), 70–83.
- Eloumala, O. P. N., Mouzong, P. M., & Ateba, B. (2014). Crustal Structure and Seismogenic Zone of Cameroon: Integrated seismic, geological and geophysical data. *Open Journal of Earthquake Research*, 3, 152–161.
- Embui, V. F., Omang, B. O., Che, V. B., Nforba, M. T., & Suh, E. C. (2013). Gold grade variation and stream sediment geochemistry of the Vaimba-Lidi drainage system, northern Cameroon (West Africa). *Natural Science*, 2013, 282–290. <https://doi.org/10.4236/ns.2013.52A040>.
- Eno Belinga, S. M. (1984). *Géologie du Cameroun: Introduction, géodynamique externe, géologie historique, géologie du pétrole* (p. 307). Yaounde: Librairie Universitaire, Université de Yaoundé.
- Essa, K. S. (2012). A fast interpretation method for inverse modeling of residual gravity anomalies caused by simple geometry. *Journal of Geological Research*, 2012, 1–10. <http://doi.org/10.1155/2012/327037>.
- Eyike, A., Werner, S. C., Ebbing, J., & Manguelle-Dicoum, E. (2010). On the use of global potential field models for regional interpretation of the West and Central African Rift System. *Tectonophysics*, 124906, 1–15. <https://doi.org/10.1016/j.tecto.2010.04.026>.
- Fan, Z., Huang, X., Tan, L., Yang, X., Zhang, H., Zhou, D., et al. (2014). A study of iron deposits in the Anshan area, China based on interactive inversion. Technique of gravity and magnetic anomalies. *Ore Geology Reviews*, 57, 618–627. <https://doi.org/10.1016/j.oregeorev.2013.09.017>.
- Faure, S. (2010). Perméabilité crustale dans le Moyen-Nord québécois: Guide d'exploration géophysique pour l'or, l'uranium et le diamant. *Rapport, Projet CONSOREM 2009–2010*.
- Faure, S., Rafini, S., & Trepanier (2009). Paléopressions, perméabilité crustale et hydrothermalisme: Implications pour les minéralisations aurifères orogéniques en Albitibi. *Rapport CONSOREM 2008-01*.
- Fishwick, S., & Bastow, I. (2011). Towards a better understanding of African topography: A review of passive-source seismic studies of the African crust and upper mantle. *The Geological Society of London*, 357, 343–371. <https://doi.org/10.1144/S1357.19>.
- Fullea, J., Fernández, M., & Zeyen, H. (2008). FA2BOUG-A FORTRAN 90 code to compute Bouguer gravity anomalies from gridded free-air anomalies: Application to the Atlantic-Mediterranean transition zone. *Computers and Geosciences*, 34(12), 1665–1681. <https://doi.org/10.1016/j.cageo.2008.02.018>.
- Goussi, G. J. F., Bisso, D., Abdelsalam, M. G., Atekwana, E. A., Katumwehe, A. B., & Ekodeck, G. E. (2017). Geophysical imaging of metacratonization in the northern edge of the Congo craton in Cameroon. *Journal of African Earth Sciences*, 2017, 1–13. <https://doi.org/10.1016/j.jafrearsci.2016.12.010>.
- Isseini, M. (2011). Croissance et différenciation crustales au Néoprotérozoïque: Exemple du domaine panafricain du Mayo Kebbi au Sud-Ouest du Tchad. Thèse de Doctorat, Université Henri Poincaré, Nancy I (France).
- Jaffal, M., El Goumi, N., Kchikach, A., Aifa, T., Khattach, D., & Manar, A. (2010). Gravity and magnetic investigations in the Haouz basin, Morocco: Interpretation and mining implications. *Journal of African Earth Sciences*, 58, 331–340. <https://doi.org/10.1016/j.jafrearsci.2010.03.012>.

- Jones-Cecil, M. (1995). Structural controls of Holocene reactivation of the Meers fault, southwestern Oklahoma, from magnetic studies. *Geological Society of America Bulletin*, 107, 98–112.
- Koch, P. (1959). Carte géologique de reconnaissance du Cameroun au 1/500000ème. Feuille NC 33 SO 0 52 Garoua-Ouest, avec notice explicative. *Publication de la Direction des Mines et de la Géologie du Cameroun*. Imprimerie Nationale, Yaoundé-Cameroun.
- Kouske, A. P., Suh, C. E., Ghogomu, R. T., & Ngako, V. (2012). Na-Metasomatism and Uranium Mineralization during a Two-Stage Albitization at Kitongo, Northern Cameroon: Structural and Geochemical Evidence. *International Journal of Geosciences*, 3, 258–279. <https://doi.org/10.4236/ijg.2012.31028>.
- Kusnir, I. (1995). Géologie, ressources minérales et ressources en eau du Tchad. CNAR, Ndjaména 2ème édition. et une carte.
- Kusnir, I., & Moutaye, H. A. (1997). Ressources minérales du Tchad: une revue. *Journal of African Earth Sciences*, 24, 549–562.
- Laplaine, L. (1968). Carte minière et des indices du Cameroun à 1/2.000.000. IGN Paris.
- Lawther, S. E. M., Dempster, T. J., Sipton, Z. K., & Boyce, A. J. (2016). Effective crustal permeability controls fault evolution: An integrated structural, mineralogical and isotopic study in granitic gneiss, Monte Rosa, northern Italy. *Tectonophysics*, 690(2016), 160–173. <https://doi.org/10.1016/j.tecto.2016.07.010>.
- Le Fur, Y. (1971). Les indices de cuivre du groupe volcanosédimentaire de Poli (Cameroun). *Bulletin Bureau Géologiques Minières*, 2ème série, section II (6), 79–91.
- Lerouge, C., Bouchot, V., & Guerrot, C. (2000). Fluids and the W (+As, Au) ore deposits of the Enguialès-Leucamp district, La Châtaigneraie, French Massif Central. *Journal of Geochemical Exploration*, 69–70(2000), 343–347.
- Leseane, K., Atekwana, E. A., Mickus, K. L., Abdelsalam, M. G., Shemang, E. M., & Atekwana, E. A. (2015). Thermal perturbations beneath the incipient Okavango Rift Zone, northwest Botswana. *Journal of Geophysical Research: Solid Earth—Wiley Online Library*, 120, 1210–1228. <https://doi.org/10.1002/2014JB011029>.
- Louis, P. (1970). *Contribution géophysique à la connaissance géologique du bassin du Lac Tchad* (p. 308). Paris: Mémoires ORSTOM.
- Marcel, J., Abate Essi, J. M., Njandjock Nouck, P., Meli'I, L. J., Mahamat, A., & Manguelle-Dicoum, E. (2018a). Geodynamic insights of the Cameroon Volcanic Line (Western Africa) from isostatic gravity anomalies. *Journal of Geodynamics*, 121, 36–48. <https://doi.org/10.1016/j.jog.2018.07.002>.
- Marcel, J., Abate Essi, J. M., Njandjock Nouck, P., Oumarou, S., & Manguelle-Dicoum, E. (2018b). Validation of gravity data from the geopotential field model for subsurface investigation of the Cameroon Volcanic Line (Western Africa). *Earth, Planets and Space*, 70(42), 1–18. <https://doi.org/10.1186/s40623-018-0812-x>.
- Maurin, J. C., & Guiraud, R. (1990). Relations entre tectonique et sédimentation dans les bassins Barrémo-Aptiens du Nord-Cameroun. *Comptes Rendus Geoscience Paris*, 308, 782–792.
- Maus, S., & Dimri, V. P. (1995). Depth estimation from the scaling power spectrum of potential fields? *Geophysical Journal International*, 124(1), 113–120.
- Mbagedje, D. (2015). Métallogénie de l'or et de l'uranium dans le cadre de la croissance et de la différenciation de la croûte au Néoprotérozoïque: Exemple du massif du Mayo-Kebbi (Tchad) dans la Ceinture Orogénique d'Afrique Centrale. These doct Univ Lorraine.
- Naidu, P. S. (1968). Spectrum of the potential field due to randomly distributed sources. *Geophysics*, 33, 337–345.
- NGA (Northwest Geophysical Associates). (2004). Gravity/magnetic modeling software GM-SYS, User's Guide.
- Ngako, V., Affaton, P., & Njonfang, E. (2008). Pan-African tectonics in northwestern Cameroon: Implications for the history of western Gondwana. *Gondwana Research*, 14, 509–522. <https://doi.org/10.1016/j.gr.2008.02.002>.
- Ngako, V., Jegouzo, P., & Soba, D. (1989). Déformation et métamorphisme dans la chaîne Pan-Africaine de Poli (Nord Cameroun): Implications géodynamiques et paléogéographiques. *Journal of African Earth Sciences*, 9, 541–555.
- Ngako, V., Njonfang, E., & Nnange, J. M. (2006). The North-South Paleozoic to Quaternary trend of alkaline magmatism from Niger-Nigeria to Cameroon: Complex interaction between hotspots and Precambrian faults. *Journal of African Earth Sciences*, 45, 241–256. <https://doi.org/10.1016/j.jafrearsci.2006.03.003>.
- Ngatchou, H. E., Liu, G., Tabod, C. T., Wang, Y., Kamguia, J., Nguiva, S., et al. (2014). Crustal structure beneath Cameroon from EGM2008. *Geodesy and Geodynamics*, 5(1), 1–7.
- Ngounouno, I., Déruelle, B., Demaiffe, D., & Montigny, R. (1997). New data on the Cenozoic volcanism of the Garoua valley (Upper Benue trough, northern Cameroon). *Comptes rendus Geoscience Paris*, 325, 87–94.
- Njel, U. O. (1986). Paléogéographie d'un segment de l'orogénèse panafricaine: la ceinture volcano-sédimentaire de Poli (Nord Cameroun). *Comptes rendus Geoscience Paris*, 303, 1737–1742.
- Nolla, J. D., Hell, J. V., Ngos, S., III, Bessong, M., Mfoumbeng, M. P., Eyong Takem, J., et al. (2015). Lithostratigraphy of the Koum Basin (Northern Cameroon). *International Journal of Multidisciplinary Research and Development*, 2(6), 103–114.
- Oesterlen, M., & Vetter, U. (1986). Petrographic-geochemical characteristics and genesis of an Albitized uraniferous granite in northern Cameroon, Africa "Vein type Uranium deposit". *IAEA, Vienna, IAEA-TECDOC-*, 361, 113–142.
- Pavlis, N. K., Holmes, S. A., Kenyon, S. C., & Factor, J. K. (2008). An Earth Gravitational Model to degree 2160: EGM2008. *Presented at the EGU General Assembly*, Vienna, Austria, April (pp. 13–18).
- Pavlis, N. K., Holmes, S. A., Kenyon, S. C., & Factor, J. K. (2012). The development and evaluation of the Earth gravitational model 2008 (EGM2008). *Journal Geophysical Research*, 117, 1–38. <https://doi.org/10.1029/2011JB008916>.
- Pawlowski, R. S. (1994). Green's equivalent-layer concept in gravity band-pass filter design. *Geophysics*, 59, 69–76.
- Pawlowski, R. S. (1995). Preferential continuation for potential-field anomaly enhancement. *Geophysics*, 60, 390–398.
- Penaye, J., Kröner, A., Toteu, S. F., Van Schmus, W. R., & Doumngang, J. C. (2006). Evolution of the Mayo Kebbi Region as Revealed by Zircon Dating: An Early (ca. 740 Ma) Pan-African Magmatic Arc in Southwestern Chad. *Journal of African Earth Sciences*, 44, 530–542. <https://doi.org/10.1016/j.jafrearsci.2005.11.018>.
- Phillips, J. D. (1998). Processing and Interpretation of Aeromagnetic Data for the Santa Cruz Basin—Patahonia Mountains Area, South-Central Arizona. *U.S. Geological Survey Open-File Report*, Arizona (pp. 02–98).
- Pinna, P., Calvez, J. Y., Abessolo, A., Angel, J. M., Mekoulou-Mekoulou, T., Mananga, G., et al. (1994). Neoproterozoic Events in the Tcholliré Area, Pan African Crustal Growth and Geodynamics in Central-Northern Cameroon (Adamawa and North Provinces). *Journal of African Earth Sciences*, 4, 347–353. [https://doi.org/10.1016/0899-5362\(94\)90074-4](https://doi.org/10.1016/0899-5362(94)90074-4).
- Pinna, P., Edimo, A., Jézéquel, J., Tchountchou, D., & Ebotayuk-Ebop, M. (1989). Inventaire minier du Centre-Nord Cameroun, (troisième phase). *Open-file Report 88 CMR 168*. Bureau de Recherches Géologiques et Minières, France.
- Poulet, A., Vidal, M., Doumngang, J. C., Vicat, J. P., & Tchameni, R. (2006). Neoproterozoic crustal evolution in southern

- Chad: Pan-African ocean basin closing, arc accretion and late- to post-orogenic granitic intrusion. *Journal of African Earth Sciences*, 44, 543–560.
- Poudjom, D. Y. H. (1993). Apport de la Gravimétrie à l'étude de la Lithosphère continentale et implications géodynamiques. Etude d'un bombement intraplaque: Le massif de l'Adamoua (Cameroun). Thèse de Doct/Ph.D, *Université Paris-Sud*, Centre d'Orsay. N° d'ordre 2798, Ed. ORSTOM.
- Rabeau, O. (2009). Distribution de l'or de type orogénique le long de grands couloirs de déformation Archéens: Modélisation numérique sur l'exemple de la ceinture de l'Abitibi. *Thèse de l'Institut National Polytechnique de Lorraine-Université du Québec*.
- Radhakrishna, I. V., & Krishnamacharyulu, S. K. G. (1990). Polyfit: A Fortran 77 Program to fit a Polynomial of any order to Potential Field Anomalies. *Journal of the Association of Exploration Geophysicists*, 2, 99–105.
- Rasmussen, R., & Pedersen, L. B. (1979). End corrections in potential field modeling. *Geophysical Prospecting*, 27, 749–760.
- Reid, A. B., Allsop, J. M., Granser, H., Millet, A. J., & Somerton, I. W. (1990). Magnetic interpretation in three dimensions using Euler deconvolution. *Geophysics*, 55, 180–191.
- Reyment, R. A., & Dingle, R. V. (1987). Paleogeography of Africa during the Cretaceous Period. *Palaeogeography, Palaeoclimatology, Palaeoecology*, 59, 93–116.
- Schwoerer, P. (1962). Carte géologique de reconnaissance du Cameroun au 1/500000ème. Feuille NC 33 SO 0 53 Garoua-Est avec notice explicative. Publication de la Direction des Mines et de la Géologie du Cameroun. Imprimerie Nationale, Yaoundé Cameroun.
- Spector, A., & Grant, F. S. (1970). Statistical models for interpreting aeromagnetic data. *Geophysics*, 135, 2983–3002.
- Stuart, G. W., Fairhead, J. D., & Dorbath, L. (1985). A seismic refraction study of the crustal structure associated with the Adamawa Plateau and Garoua rift, Cameroon, West Africa. *Geophysical Journal of the Royal Astronomical Society*, 81, 1–12.
- Tchameni, R., Doumngang, J. C., Deudibaye, M., & Branquet, Y. (2013). On the occurrence of gold mineralization in the Pala Neoproterozoic formations, South-Western Chad. *Journal of African Earth Sciences*, 84, 36–46.
- Telford, W. M., Geldart, L. P., & Sheriff, R. E. (1990). *Applied geophysics* (2nd ed.). Cambridge: Cambridge University Press.
- Tenthorey, E., & Fitz Gerald, J. D. (2006). Feedbacks between deformation, hydrothermal reaction and permeability evolution in the crust: Experimental insights. *Earth & Planetary Science Letters*, 247(2006), 117–129. <https://doi.org/10.1016/j.epsl.2006.05.005>.
- Thomson, D. T. (1982). A new technique for making computer-assisted depth estimates from magnetic data. *Geophysics*, 47, 31–37.
- Tokam, A. P., Tabod, C. T., Nyblade, A. A., Jordi, J., Wiens, D. A., & Pasyanos, M. E. (2010). Structure of the crust beneath Cameroon, West Africa, from the joint inversion of Rayleigh wave group velocities and receiver functions. *Geophysical Journal International*, 183, 1061–1076.
- Toteu, S. F., Penaye, J., Deloule, E., Van Schmus, W. R., & Tchameni, R. (2006). Diachronous Evolution of Volcano-Sedimentary Basins North of the Congo Craton, Insights from U-Pb ion Microprobe Dating of Zircons from the Poli, Lom and Yaounde' Groups (Cameroon). *Journal of African Earth Sciences*, 44, 428–442. <https://doi.org/10.1016/j.jafrearsci.2005.11.011>.
- Toteu, S. F., Penaye, J., Deschamps, Y., Maldan, F., Nyama Atibagoua, B., Bouyo, et al. (2008). Géologie et ressources minérales du Cameroun 1/1.000.000. In 33rd *International Congress*, Oslo, Norway, August 2008, (pp. 6–14).
- Toteu, S. F., Penaye, J., & Poudjom, D. Y. H. (2004). Geodynamic evolution of the Pan-African belt in central Africa with special reference to Cameroon. *Canadian Journal of Earth Sciences*, 41, 73–85. <https://doi.org/10.1139/E03-079>.
- Toteu, S. F., Van Schmus, W. R., Penaye, J., & Michard, A. (2001). New U-Pb and Sm-Nd data from north-central Cameroon and its bearing on the Pre-Pan-African history of Central Africa. *Precambrian Research*, 108, 45–73. [https://doi.org/10.1016/S0301-9268\(00\)00149-2](https://doi.org/10.1016/S0301-9268(00)00149-2).
- Van Schmus, W. R., Oliveira, E. P., Da Silva Filho, A. F., Toteu, S. F., Penaye, J., & Guimarães, I. P. (2008). Proterozoic links between the Borborema Province, NE Brazil, and the Central African Fold Belt. *The Geological Society of London*, 294, 69–99. <https://doi.org/10.1144/SP294.5>.
- Wolfgang, J., & Smilde, P. L. (2009). *Gravity interpretation: Fundamentals and application of gravity inversion and geological interpretation*. Berlin: Springer.
- Won, I. J., & Bevis, M. (1987). Computing the gravitational and magnetic anomalies due to a polygon: Algorithms and Fortran subroutines. *Geophysics*, 52, 232–238.
- Yushan, Y., & Yuanyuan, L. (2017). Crustal structure of the Dabie orogenic belt (eastern China) inferred from gravity and magnetic data. *Tectonophysics*, 17, 1–17. <https://doi.org/10.1016/j.tecto.2017.12.016>.